PATH PLAN PERFORMANCE EVALUATION OF THE CHALLENGE 1: A SMALL UNMANNED SURFACE VEHICLE FOR RADIATION DETECTION AND MAPPING

A Thesis

by

GRANT ANDREW WILDE

Submitted to the Office of Graduate and Professional Studies of
Texas A&M University
in partial fulfillment of the requirements for the degree of

MASTER OF SCIENCE

Chair of Committee,	Robin R. Murphy
Committee Members,	Dylan A. Shell
	Craig M. Marianno
Head of Department,	Dilma Da Silva

August 2016

Major Subject: Computer Science

ABSTRACT

This thesis will compare the performance of the Challenge 1 unmanned surface vehicle when autonomously conducting a radiological survey of a bounded, obstacle free, convex polygon via a traditional raster scan versus a novel spiral-like path plan. Currently, unmanned ground vehicles (UGV), unmanned aerial vehicles (UAV), and unmanned surface vehicles (USV) use a simple raster scan to insure complete coverage of a predefined, obstacle free area. Raster scans require a 180 degree change in heading which is easy for tracked UGVs and vertical take-off UAVs to accomplish, but more difficult for marine vehicles and fixed winged UAVs. A spiral-like path plan will not completely eliminate turns close to 180 degrees, but presents the possibility of removing the number of sharp turns at the expense of adding more slight turns. The author of this thesis originally hypothesized that this spiral-like path plan would result in shorter autonomous surveys by the Challenge 1 USV, as well as a higher percentage of coverage. Shorter surveys will allow operators such as the mission specialist overseeing a disaster in which radiological material may be present or treaty verification inspectors searching a facility to conduct more surveys in a limited time, which therefore increases the total area searched over this time period as well as provides data to the mission specialist faster. A higher percentage of coverage attained by the spiral-like path plan would guarantee a more complete representation of the area surveyed.

To test this hypothesis the author used the 1.15 acre pond at John Crompton Park in College Station, Texas, to generate twenty-five unique convex polygons via teleoperation of the Challenge 1, ranging in size from 450 square meters to 1027 square meters, to which a raster path plan and spiral-like path plan were each used

by the Challenge 1 to survey the area, resulting in fifty total runs. Following the data collection, the associated log from each run was used to calculate total survey time, total survey distance, root mean square of cross-track error, Hausdorff Distance (max RMS error), percent coverage, and percent of survey locations inside the bounded convex polygon. The average survey time for a spiral like path plan versus a raster scan was 13.68 seconds shorter ($p < .59$). The average total distance for a raster path versus a spiral like path was 15.53 meters less ($p < .061$). The average RMS of cross-track error for a spiral like path plan versus a spiral path plan was 0.31 meters less ($p < .123$). The average Hausdorff Distance for a spiral like path plan versus a raster scan was 1.53 meters less ($p < 0.0005$). The average of percent coverage for a raster scan versus a spiral like path was 4.22% higher ($p < 0.027$). The average of percentage of locations in the bounding area for a raster path versus a spiral like path was 16.88% higher ($p < 0.00023$). This shows that for $\alpha = .05$, there is no statistical difference between either of the two path plans for survey time, survey distance, or RMS of cross-track error. However, there is a statistical difference between the two path plans for Hausdorff Distance, percent coverage and percentage of locations inside the bounding area. Due to the spiral path plan's inability to maintain locations inside the bounding area, a raster scan is the best path plan to use when surveying a bounded convex polygon with the Challenge 1 since it results in the highest percentage of coverage with no statistical difference in survey time, survey distance, or RMS of cross-track error. This result is only guaranteed for the Challenge 1 and its associated controller, with potentially different outcomes if tested on other surfaces vehicles, especially those with underwater propellers, rudders, or jet pump (no propeller or rudder) propulsion systems.

DEDICATION

I dedicate this thesis first and foremost to our Heavenly Father. I am extremely blessed to have the opportunity to pursue a graduate degree at Texas A&M, and this is all possible because of Him. Next I dedicate this thesis to my loving wife, Emily Wilde, my supportive parents, Ben and Betsy Wilde, my sister Kate Barnett, as well as the rest of my extended family and friends. Without your support, I would never have completed this project.

ACKNOWLEDGEMENTS

I wish to express my sincere appreciation to my family for allowing me to continue my education and for their support while working on this project.

I am grateful to Dr. Robin R. Murphy, my committee chairman, for her instruction and guidance throughout this project. I am also grateful to the other members of my committee, Dr. Dylan A. Shell and Dr. Craig M. Marianno, for their suggestions and constructive criticism of this thesis.

I would like to thank my fellow labmates: Traci Sarmiento, Brittany Duncan, Jesus Suarez, Siddharth Agarwal, Khuong Nguyen, Jan Dufek, Xuesu Xiao, and Gino Chacon for their suggestions and opinions in helping me complete my class work and this manuscript.

To Eric Cochrane, Joshua Deitche, Gregory Donelan, Timothy Jacomb-Hood, Ishita Mandhan, Michael Marmo, Daniel Murchison, Rebecca Schofield, and Tianyi Zhang, thank you for your hard work during the 2014-2015 AggiE Challenge Project.

A special thanks to the personnel at Texas A&M Extension Service's (TEEX) Disaster City, especially Clint Arnett for allowing me to conduct trials at their facility, and to the City of College Station for allowing me to conduct my experiments at John Crompton Park.

Portions of this work were supported by The United States State Department and Sandia National Labs. I would like to thank the Dwight Look College of Engineering at Texas A&M University for sponsoring the AggiE Challenge which allowed me to be a teaching assistant for one of its projects.

NOMENCLATURE

CRASAR	Center for Robot Assisted Search and Rescue
DF	Degrees of Freedom
EMILY	Emergency Integrated Lifesaving Lanyard
OCU	Operator Control Unit
PI	Proximity Index
PWM	Pulse Width Modulation
RMS	Root Mean Square
SUAS	Small Unmanned Aerial System
TEEX	Texas A&M Engineering Extension Service
UAV	Unmanned Aerial Vehicle
UGV	Unmanned Ground Vehicle
USSV	Unmanned Semisubmersible Vehicle
USV	Unmanned Surface Vehicle
UTM	Universal Transverse Mercator

TABLE OF CONTENTS

Page

LIST OF FIGURES

FIGURE Page

LIST OF TABLES

TABLE Page

1. INTRODUCTION*

Man packable unmanned surface vehicles can be used for nuclear treaty verification, rapid assessment of nuclear emergencies, and monitoring recovery from a nuclear accident. After the first use of a nuclear weapon by the United States on August 6, 1945, the United States, Russia, the United Kingdom, France, China, India, Pakistan, Israel and North Korea possess approximately 17,200 nuclear weapons [15]. Beginning with the Partial Test Ban Treaty and continuing through the Comprehensive Test Ban Treaty, there have been treaties pushing for the disarmament and reduction of nuclear stock piles. As an alternative to cooling towers, nuclear warhead producing facilities are often in close proximity to a cooling pond. Cooling ponds are used instead of direct discharge of heated water to a nearby river or bay. This provides the opportunity for unmanned marine vehicle (UMV) systems to facilitate inspectors in determining through radiation sampling whether a certain facility is in fact dismantling warheads or creating wards without having to physically enter the site. UMVs can also be used during nuclear emergencies. For example, the explosion at the Chernobyl nuclear facility on April 26, 1986, released large quantities of nuclear fuel and radionuclides from the fission products that were being created. Chernobyl used cooling ponds which proved a means of radiation sampling without entering the facility. UMV sampling would not be possible in all cases, considering that the Fukushima Daiichi plants used cooling towers and pumped water to sea.

The first known man-packable unmanned surface vehicle (USV) system designed for radiation localization in shallow waters for nuclear treaty verification or sampling

*Part of this section is reprinted with permission from G. A. Wilde, R. R. Murphy, D. A. Shell, and C. M. Marianno. A man-packable unmanned surface vehicle for radiation localization and forensics. In 2015 IEEE International Symposium on Safety, Security, and Rescue Robotics (SSRR), pages 1-6, Oct 2015. Copyright[2015] by IEEE.

after a nuclear incident was developed by Wilde et al. in 2015 [28]. The created system consisted of the Challenge 1 USV which is a Lutra 1.1 autonomous airboat modified to carry an UltraRadiac^{TM}-Plus Personal Radiation Monitor. Radiation sensing is noisy and a reading at a single point may not reflect the overall radiation in the area. To combat this problem, areas are sampled rather than a single point taken. The debris-free area that is to be surveyed is determined by teleoperation so that the operator can visually verify the area is safe to survey. Once the bounded area is determined, the Challenge 1 then explores the area via a novel, spiral-like path rather than a traditional boustrophedon path, aka a raster scan. Radiation readings are taken and stored locally onboard the USV throughout the boundary marking and autonomous survey. After the autonomous survey is complete, the data can be removed and analyzed. The sampled area is most likely going to result in survey data that is widely varying and difficult for humans to interpret. With this said, the data collected can be interpolated which in turn can be used to form a visual heatmap that reliably portrays the smoothed data. For more information on each of the three main components of the created Challenge 1 System as well as an analysis of the its first test with an active radiation source, see Appendix 1.

The initial test of the Challenge 1 USV System brought rise to the motivating problem: "When using an unmanned surface vehicle to conduct a radiological survey of a bounded, obstacle free convex polygon, what is the best path plan to use?" When given limited time to make the correct decision regarding a potentially radioactive area, mission specialists following a nuclear disaster or treaty verification inspectors have to be confident that the field robot being used will survey the area to the best of its ability. Traditionally, robots use a raster scan to survey the area in question. However, it is unknown if this is the best path plan to use or if there is a potentially better alternative in existence. In order to solve this motivating problem, this thesis

will address the following research question: *Is a novel, spiral-like path plan better than a raster scan for a USV when conducting a survey of a bounded, obstacle free polygon?* Using a spiral-like path plan with an unmanned marine vehicle is a novel research area as is the metrics used to compare unmanned marine vehicle paths. In order to answer this research question, five further questions must be answered as well, those being:

1. Which path plan results in the shortest survey time carried out by the robot?
2. Which path plan results in the shortest path length carried out by the robot?
3. Which path plan results in the lowest root means square of cross-track error?
4. Which path plan results in the lowest Hausdorff distance, a measure of the maximum distance the vehicle reached from the intended path?
5. Which path plan results in a greater percentage of coverage?

The purpose of this thesis is to quantitatively determine which path plan, either the novel spiral-like path plan or the traditional raster scan, results in the best survey of the Challenge 1 USV System when conducting a survey of a bounded, obstacle free convex polygon. The two primary contributions provided by this thesis work to the fields of unmanned marine robotics, first responders, and mission specialists are: i) first path plan comparison of the Challenge 1 System, and ii) a novel compendium of quantitatively metrics for unmanned marine vehicle path plan comparison trials.

Contribution 1: first path plan comparison of the Challenge 1 System. This work presents the first formal study for determining whether a novel spiral-like path plan will result in better autonomous surveys conducted by the Challenge 1 versus the traditional raster scan. As seen in [28], the Challenge 1 can successfully collect

radiation readings from an active radiation source. If needed, the Challenge 1 could be used by first responders or treaty verification inspectors, but prior to this study, the best path plan for the given controller was not known.

Contribution 2: a novel compendium of quantitative metrics for unmanned marine vehicle path plan comparison trials. As will be seen in the Literature Review of this thesis, there is not a definitive set of metrics used to analyze the complete survey of an unmanned marine vehicle survey. This thesis provides five metrics, that when used in combination, can be used to determine the best path plan for a unmanned marine vehicle in regards to the total survey which includes straight segments of the path as well as portions where the vehicle is turning around.

This thesis is organized as follows. Chapter 2 serves as a review of the research literature for small unmanned marine vehicles, robotic radiation sampling, path planning, and surface vehicle experiment methodology. Presented next in Chapter 3 is the approach taken for development of the novel, spiral-like algorithm used as well as an improved raster scan. Chapter 4 details the implementation of the proposed algorithms with the Challenge 1 System. Chapter 5 describes the experimental methods and the results of this experiment. The thesis concludes with Chapter 6 where a discussion of the results is presented, as well as future work for this research project.

2. LITERATURE REVIEW

Small unmanned surface vehicles for radiation detection and localization are an active area of investigation. This section presents the literature and areas of industrial application that were surveyed to understand each component of the USV system as well as the associated experiments: small USVs for remote presence, robotic radiation sampling, path planning, and surface vehicle experiments and methodology.

The literature shows that prior to Wilde et al's work in [28], small unmanned surface vehicles have been used in at least six applications, but not for radiation sampling which is the ultimate application of this thesis. The literature did reveal that unmanned ground and aerial vehicles were used at the Fukushima Daiichi nuclear incident, but no surface vehicles were used. Unmanned vehicles have not been used at any other radiological incidents, except that of the Fukushima Daiichi incident. Of the papers surveyed pertaining to robotic radiation sampling, only [13] employed the used of an autonomous survey; all other missions were conducted via teleoperation. The literature showed that the idea of a spiral path plan is not new to the field of robotics, but the idea of a spiral-like path plan formed by shifting the edges of a convex polygon in towards the center of the polygon at a fixed, constant spacing is novel. The implementation of this spiral-like path plan with a small unmanned surface vehicle has not been seen in the literature as well. The marine vehicle experiment methodology literature revealed three metrics outside that of total time of survey and total distance of survey. Those three metrics are: RMS of cross-track error, Hausdorff distance, and area between actual path and desired path. This thesis will combine time, distance, RMS of cross-track error, Hauusdorff distance, and percent coverage in a novel way to evaluate and analyze a surface vehicle's complete

autonomous survey rather than only the straight segments of a survey which is what three of the survey papers did. By analyzing the straight segments of the survey only, considerable portions of the vehicle's survey were not accounted for if the vehicle was turning around. The combination of metrics that will be used in this thesis will account for the vehicle turning around.

2.1 Small Unmanned Surface Vehicles

Unmanned surface vehicles are not new platforms to the field of robotics. Various post World War II USV projects were mainly used as gunnery and middle target systems [8]. Since the early 1990s, USV systems have garnered more attention by the United States Navy, whose main focus is on littoral warfare and anti-terrorism missions [4]. More recently, USVs have been used for environmental monitoring. Stemimle and Hall have used a 1.9 m x 1.2 m USV equipped with a Dual frequency IDentification SONar (DIDSON) that was used to image spawning black drum [25]. The first documented use of a surface vehicle in emergency response was by Murphy et al. in 2005 when the Center for Robot Assisted Search and Rescue (CRASAR) deployed an iSENYS unmanned aerial vehicle (UAV) and a USV to survey the damage inflicted by Hurricane Wilma [18]. The USV was used to detect damage to sea walls and piers, locate underwater debris, and determine safe regions for sea navigation. Research interest in surface vehicles has focused on larger USVs, with micro-USVs having received comparatively little attention. Researchers at Carnegie Mellon's Robotics Institute have developed the Cooperative Robotic Watercraft (CRW) [27]. This surface vehicle has been released as a commercial product in the form of the Lutra Airboat which is the data collection platform that will be used in this thesis. The CRW can be equipped to take physical samples or measure other water characteristics such as depth, pH levels, electrical conductivity, temperature, and dissolved

oxygen. Hydronlalix has developed EMILY (Emergency Integrated Lifesaving Lanyard) [22]. This 11.34 kg (25 lbs) jet propelled robot equipped with a flotation device, can be used to rescue victims in deep, rough waters.

2.2 Robotic Radiation Sampling

Teleoperated unmanned ground vehicles were first used for radiation forensics and localization in Japan at the 2011 Fukushima Daiichi Nuclear Power Plant incident , [10], [19], [21]. At the Fukushima Daiichi accident, robots were used to assess the damage both indoors and outdoors, conduct radiological surveys, and help with cleanup operations [10], [19]. A QinetiQ Talon combined with a gamma radiation camera were used to localize pieces of radiological material that needed to be removed from the areas around the reactors [21]. Small unmanned aerial systems (SUAS) were deployed for the first time to a radiological disaster at the Fukushima Daiichi Nuclear Power Plant as well [17]. Two Honeywell T-Hawk unmanned aerial vehicles were used to conduct radiological surveys and assess structural integrity of buildings. Kochersberger el. al equipped an Aeroscout B1-100 SUAS with a radiation spectrometer payload used to determine gamma radiation intensity and spectrum [13]. This system was also tested with an unmanned ground vehicle that was capable of taking physical samples. Wilde et al. were the first to use a micro unmanned surface vehicle equipped with a radiological sensor for radiation detection and localization [28]. Of the papers surveyed in this section, only [13] and [28] used unmanned vehicles that autonomously surveyed a given area. All other vehicles were teleoperated by the pilot.

According to Dr. Craig Marianno, an expert in nuclear engineering, inspectors responding to a nuclear incident are concerned about two key questions: 1)Where is the source of the radiation? 2) Where are the plumes of the radiation, or in other

words, where are radiation levels too high for human inhabitance and where radiation exposure rates are low enough for humans to enter the area safely? Exposure rate $\dot{X}$ as defined in [12] is:

$$\dot{X} = \Gamma_\delta \frac{\alpha}{d^2}$$

where α is the activity of the source, Γ_δ is defined as the exposure rate constant for the specific radioisotope of interest, and d is the distance to the source. With this said, exposure rate at a particular distance d from the source will be different than the expected value if a medium or object with shielding properties is between the source and position of the reading [12]. For this reason, this thesis will focus on a path plan that could be used to both localize and map a potential radiation source.

2.3 Path Planning

The goal of robot coverage in a bounded, obstacle free environment, is to plan a path that brings the robot within a fixed distance of every point in the free space. Applications include painting, vacuuming, and floor scrubbing. This problem has been studied in depth by roboticists working with ground and aerial vehicles, with less work given to surface vehicles. Recent research has focused on the coverage problem in an obstacle filled environment. For example, Choset and Pignon developed the boustrophedon cellular decomposition method in which the area to be searched is broken into cells and each cell is covered with simple back and forth motions [7]. The orientation of said back and forth motions has typically been oriented with the longest segments of the path when conducted indoors. The outdoor used, fixed wing Precision Hawk surveys a predefined area given by a simple boustrophedon path (aka lawn mower or raster scan), but orientation is not known until flight time. Before the survey begins, the UAV performs two to three loiter laps in which wind direction is determined. Once wind direction is known, the long portions of the path are oriented

parallel to the wind so the platform does not fly perpendicular to a cross wind. Kitts et al. used a boustrophedon with their dual hull designed USV [11]. No detail was given with regards to the orientation compared to wind direction. The CRW used by Valada et al. performed a simple boustrophedon path plan, but the orientation on the long segments of the path were always oriented east to west and west to east [27]. This means, the CRW has not been intentionally oriented to travel with and against the wind. The problem seen by the author of this thesis with the Precision Hawk and path plan used in [11] is the raster scan's waste of time and energy to turn around. In both of these two examples, the U-turns take place outside the intended area to survey. This results in longer surveys that require more battery power.

The idea of using a spiral for robotic path planning is not a new idea. Ferri et al. introduce a biologically-inspired algorithm named SPIRAL (Searching Pollutant Iterative Rounding ALgorithm) [9]. In this approach the robot moves along a spiral path and stops frequently in order to sample the gas. Based on the features collected from the information acquired, the robot computes an index, called the Proximity Index (PI), to assess how close the source of the gas is to the sampling location. Based on considerations about the calculated PIs, a spiral may be reset and, after that, a new one is started. This movement allows the robot to approach an emitting source without relying on any information about the airflow. In regards to the localization problem, this algorithm appears to be an excellent candidate, but this algorithm would not be a fitting candidate for the mapping problem seeing as complete coverage of an area is not the focus of the plan. The path plan was also a true, spherical spiral, this would not work in a convex polygon.

Lilienthal et al. used a rectangular spiral path plan in their experiments to address the problem of mapping the structure of gas distribution [16]. In this strategy, the robot follows a sequence of rectangular spirals centered at the gas source. The path

consists of a sequence of inward and outward movements with a varying distance to the center. This paper only operated in a square or rectangle, in other words, the path plan was never tested on polygons with more than 4 vertices or with irregularly shaped convex polygons.

Seo et al. used a spiral motion in simulation when considering using an Unmanned Surface Vehicle for detecting dinoflagellate Cochlodinium polykrikoides, a form of red tides [26]. The spiral motion used by Seo et al. was added when the vehicle could not detect Harmful Algal Blooms (HAB) even if operating turning motion for path recovery. As previously stated, this was only performed in simulation and was used to recover the path plan. The spiral was seen to overlap and appear spherical in this paper.

2.4 Surface Vehicle Experimental Methodology

The first metric used by Kitts et al. for the evaluation of the USV path performance was cross-track error [11]. Cross-track error is the distance the vehicle is from its desired path. Results were reported as a root means square (RMS) of cross-track error. A similar metric used in [23] and [24] was Hausdorff distance. The Hausdorff distance is the maximum cross-track error throughout the survey.

The second metric seen to be used by researchers conducting USV experiments was the area between the actual and desired paths, normalized with respect to the path length. Normalized area was used in [5], [6], [23], and [24]. Normalized area is calculated as the summation of the areas of non-self-intersecting and consecutive polygons formed by the finite chain segments, i.e. the desired path and the executed path. The author of this thesis believes RMS of cross-track error to be an equivalent metric to normalized area, and therefore normalized area will not be calculated in the final results of this thesis. Percent coverage, a metric to be explained further,

will calculate how much of the intended area was surveyed and how much of the intended area was not surveyed.

The literature has shown, that researchers tend to divide a surface vehicle's path into multiple phases. For example, Bibuli et al. divided the USV maneuver into three phases: 1) U-turn 2) Transient 3) Steady state [6]. Saggini et al. divided vehicles path into: 1) Path approach 2) Path-following 3) Path connection [23]. Sorbara et al. divided each run into four sequential phases: 1) Approach 2) Forward path 3) Turn 4) Backward path [24]. In [24], performance is measured only while executing the forward path. [11] only calculated RMS of the cross-track error whenever the vehicle was in the bounded area to survey. In [23], normalized area and Hausdorff distance were only calculated for the straight portions of their lawn mower grid experiment. The author of this thesis disagrees with this philosophy due to turning around being a part of the overall survey length and time. Any and all traversing of the vehicle should be considered in the final calculations.

Kitts et al. performed seven separate missions [11]. During these missions, only wind speed was recorded. Wind was recorded in knots. Saggini et al. presented data for five separate trials [23]. Since each run was dived into on of four sequential phases, each run was therefore subdivided. Trial 1 was divided into six portions, Trial 2 was divided into four portions, Trial 3 was divided into six portions, Trial 5 was divided into ten portions, and Trial 5 was divided into thirteen portions. For each portion, normalized area, Hausdorff distance (Max RMS), and RMS were presented. Sorbora et al. presented data for twenty total trials [24]. Ten of the trials were conducted on Charlie USV and ten trials on on the Shark USSV (Unmanned Semisubmersible Vehicle). For each of the twenty trials, normalized area and Hausdorff distance were presented. Bibuli et al. ran forty different phases [6]. Since a trial is divided into multiple phases, it is not clear how many separate trials were ran. In [5], two different

path plans were tested with area and normalized area presented for each of the two paths.

This thesis will combine total survey time, total survey distance, RMS of cross-track error, Hausdorff distance, and percent coverage into a new set of performance metrics. These metrics will be applied to every segment of the vehicle's path. This includes straight segments as well as segments incurred in turning maneuvers. Since the main focus of this thesis is to quantitatively compare two different path plans, all portions of the survey must be accounted for, especially since the turning maneuvers associated with each path plan could affect the survey as a whole.

3. APPROACH

This section begins by detailing the motivation for the spiral-like path plan used in this thesis as well as explains the spiral-like algorithm itself. It is important to note, that this path plan is referred to in this thesis as "spiral-like" due to the fact that the path plan is not a perfect spiral, as would be seen in the Archimedean Spiral (Figure 3.1). Instead, this algorithm is based on the idea of moving the bounding polygon's edges in towards the centroid at a fixed distance, resulting in turns that are not as smooth as the Archimedean Spiral, but at the same time having a spiral or looping effect similar to that of a perfect Archimedean spiral. Following the explanation of the spiral-like path plan algorithm, this section details the use of a rotation matrix to orient the transects of a traditional raster scan with and against the wind. This section concludes with how each of the six metrics computed in this study could be calculated for any arbitrary surface vehicle survey.

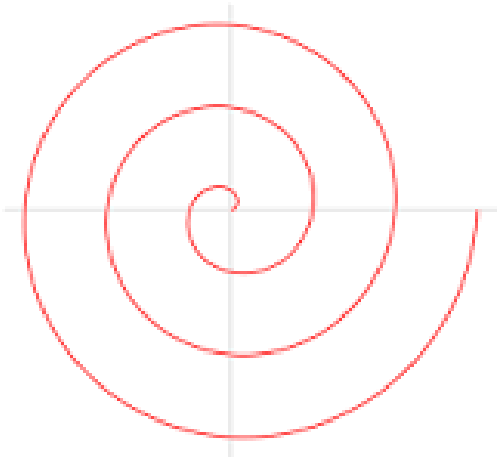

Figure 3.1: An example of an Archimedean spiral.

3.1 Spiral-like Path Plan

The author's motivation for a spiral-like path plan came from agricultural practices of the drought stricken area of West Texas. Due to the area's low annual rainfall, center pivots are the most common form of crop irrigation. Center pivots offer a method of irrigation in which an irrigation pipe with sprinklers positioned along its length are mounted to motorized, wheeled towers. The center pivot is fixed to the ground at its central location and allowed to rotate, or pivot about the center, which in turn allows a circular area to be watered. Center pivots can be moved from one central location, to another, allowing multiple areas to be water by one pivot and for an equipment free, circular section of the field to be maintained during the farming season. With recent advances in precision agriculture, self-driven tractors have been used in combination with spiral path plans to plow, plant, spray, and harvest the area under center pivots. A spiral path plan allows a farmer to set his plow down onto the ground at the beginning, outer edge of the field and plow continuously, without having to turn around, until he reaches the center. This continuous movement allows the farmer to save precious time versus the traditional raster scan since the raster scan requires a farmer to lift up his implement, make a 180 degree change in heading, and place the implement back down at each end of the field. This spiral path plan will only work for true circles, in other words, not an irregular bounded area. After the n boundary points have been marked, the following algorithm will be called:

1. Connect n-1 many points to form n-1 many line segments. The line segment that is left unconnected is from boundary point n to 1.
2. Add all the points 1, 2,..., n to the newPath list.
3. Create n-1 many parallel line segments towards the inside of the polygon with

a spacing d, and store them in an array. There is a parallel line for each of the line segments formed from Step 1.

4. Find the angle theta between the boundary points 1, 2, and n.
5. Draw a line at theta/2 from the line segment formed by boundary points 1 and 2, with the new line running through boundary point 1.
6. Intersect the line drawn from Step 5 with the line segment parallel to boundary points 1 and 2 formed in Step 3.
7. Add this new point to the newPath list.
8. Create a new line segment from point n to the point from Step 7.
9. Create a new parallel line towards the inside of the polygon with a spacing d from the line segment formed in Step 8. and store in array. // Initialization is now complete now begin an iterative process with loopCounter = 0
10. Find the intersection of the parallel lines stored at array[loopCounter] and array[loopCounter+1].
11. Add this point to newPath list
12. Draw a line from the second to last waypoint in the list to the new point generated in Step 10.
13. Create a line parallel to the line created in Step 12 that is d units towards the inside of the polygon and add to the array.
14. Increment loopCounter.
15. If this new line segment is less than d units away from the centroid, add the centroid as the final path to traverse to and break from the loop. Else, return to step 10. This concludes the new spiral-like path planning algorithm.

An example of the spiral path planning algorithm is below.

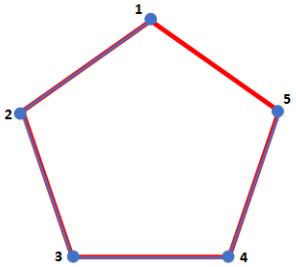

(a) Spiral Algorithm Steps 1-2

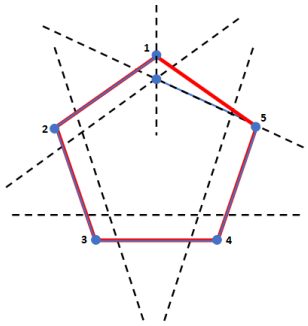

(b) Spiral Algorithm Steps 3-8

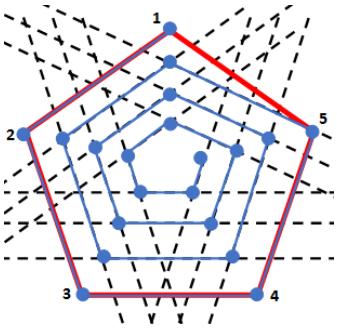

(c) Spiral Algorithm Steps 10-14

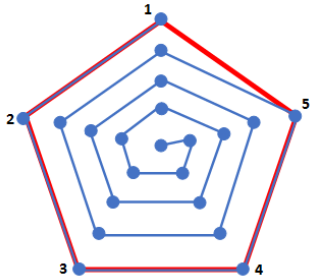

(d) Spiral Algorithm Step 15

Figure 3.2: A visual representation of the implemented novel spiral path algorithm on a bounded regular polygon.

The red polygon in the above figures is the original bounding area of the section to be surveyed, the blue circles are waypoints the USV is to traverse to, the black dashed lines are shifted parallel line segments, and the blue line segments indicate the path the USV should follow while traversing to the next waypoint in the list.

Following the above algorithm, one can see that first, each vertex of the polygon is added to the path (Figure 3.2a). Then vertex 1 is divided in half as shown by the vertical dashed line. Next the intersection of the vertical line and shifted parallel line formed by vertices 1 and 2 is found, and this new point is added to the path (Figure

3.2b). This concludes step 9 from above and initialization is now complete. Now steps 10 through 14 are completed as long as the distance from any newly added line segment to the centroid is less than the transect distance d (Figure 3.2c). When a line segment is noted as being less than d units to the centroid, the loop breaks, and the centroid is added as the final waypoint to traverse to (Figure 3.2d).

3.2 Raster Scan Path Plan

The algorithm used to create a wind oriented raster scan has three phases: 1) Initial rotation of bounding polygon 2) Raster scan waypoint generation 3) Post rotation of generated waypoints back to the correct orientation. For this algorithm a *wind heading (wh)* parameter is used to orient the transects of the path plan parallel to the wind direction. A complete description of the raster scan path planning algorithm is below:

1. Rotate the given bounding polygon by multiplying each point by the below rotation matrix:
$$\begin{bmatrix} \cos\theta & -\sin\theta \\ \sin\theta & \cos\theta \end{bmatrix}$$

2. Compute a bounding rectangle around the rotated bounded area by computing minLat, minLong, maxLat, maxLong. The vertices of the bounding rectangle are as follows: (minLong,minLat), (minLong,maxLat), (maxLong,maxLat), (maxLong,minLat)

3. Starting with the minLong add horizontal, parallel line segments up towards the maxLong

4. Find the intersection of all bounding edges of the rotated polygon with the newly added line segments.

5. Sort the list of all intersections from minimum latitude to maximum latitude.

6. Add the first intersection to the path and remove from the list.

7. Remove the next two points from the list and store them as Point1 and Point2 respectively.

8. Calculate the distance from Point1 and Point2 to the first waypoint added to the path and store them as distance1 and distance2 respectively.

9. If distance1¡distance2, then add Point1 to the the path, then Point2. Else add Point2 to the path, then Point1.

10. Compare the longitude's of the very first point added the the path to that of the very last point added to the path at this time. If the last coordinate added has a longitude less than the first coordinate added, set the variable isLeft=true, else set isLeft=false.

11. While the size of the sorted intersection list is not equal to zero, do the following steps:

12. Remove the next two points from the sorted intersection list and sort them according to their longitude into leftPoint and rightPoint so that leftPoint's longitude is less than rightPoint's longitude

13. If isLeft==true add the points leftPoint and rightPoint to the path in that order and set isLeft=false. Else, add the points rightPoint and leftPoint in that order and set isLeft=true.

14. Once the list containing all the sorted intersections is empty, rotate each point

by the below matrix. This step rotates our path back to the correct orientation.

$$\begin{bmatrix} \cos\theta & \sin\theta \\ -\sin\theta & \cos\theta \end{bmatrix}$$

A visual diagram of the above algorithm is presented below.

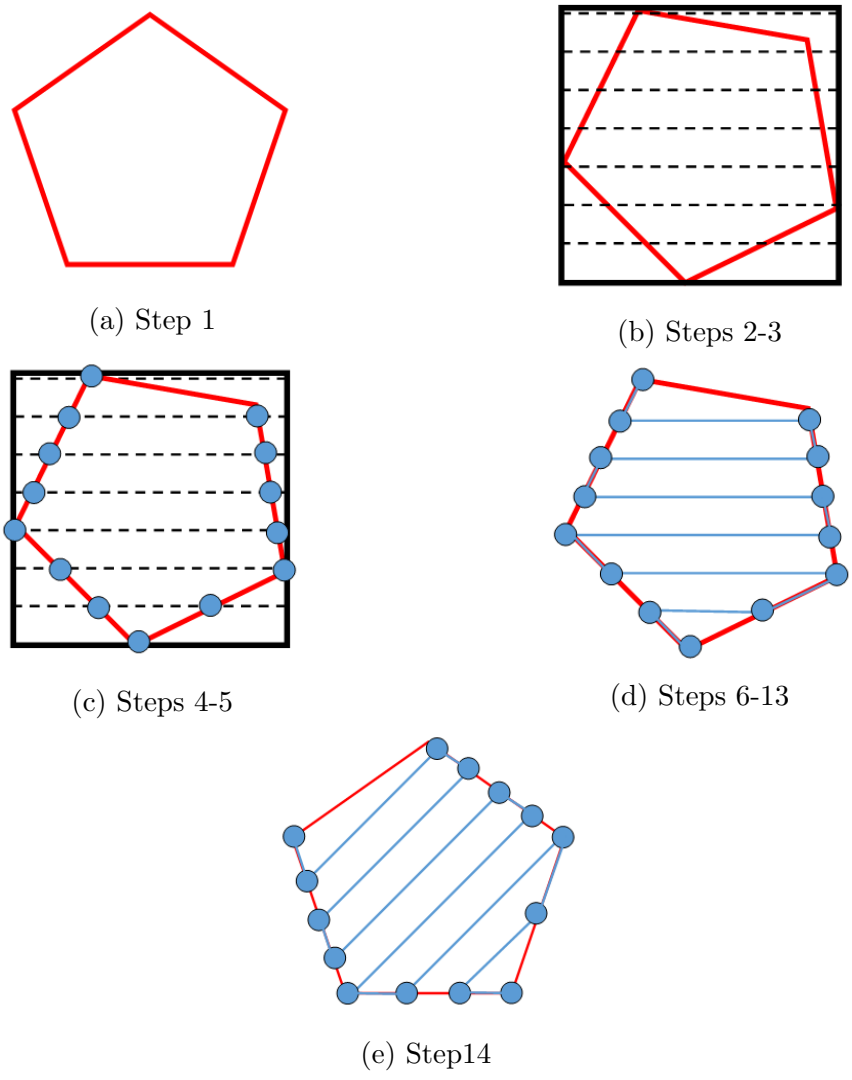

(a) Step 1

(b) Steps 2-3

(c) Steps 4-5

(d) Steps 6-13

(e) Step14

Figure 3.3: A visual representation of the implemented raster scan path algorithm on a bounded regular polygon.

The red polygon in the above figures is the original bounding area of the section to be surveyed, the blue circles are waypoints the USV is to traverse to, the black dashed lines are horizontal line segments extending from the far left of the bounding box to the far right of the bounding box, and the blue line segments indicate the path the USV should follow while traversing to the next waypoint in the list.

Following the above algorithm, one can see that the original bounding area to be surveyed (Figure 3.3a) is rotated by the wind direction parameter, which in this case is 45 degrees and horizontal line segments beginning at the minimum longitude and extending up to the maximum longitude (Figure 3.3b). Each of the horizontal line segments are evenly spaced with a distance of d units. Next, each intersection of a horizontal line segment and any of the intended, rotated bounded edges is found (Figure 3.3c). Once each intersection has been found, Steps 6-13 are executed as to form the rotated path. Following the completion of the rotated path, the waypoints are then rotated clockwise by the wind parameter, which results in a raster scan with parallel transects oriented at 45 degrees.

3.3 Measures

As stated in the Introduction section, this thesis will answer the following questions in regards to the Challenge 1's survey when carried out by an autonomous spiral-like path plan versus a traditional path plan:

1. Which path plan results in the shortest survey time carried out by the robot?
2. Which path plan results in the shortest path length carried out by the robot?
3. Which path plan results in a lower root means square of cross-track error?
4. Which plan results in a lower Hausdorff distance?
5. Which path plan results in a greater percentage of coverage?

In order to answer each of the above questions, data from the survey must be logged for post survey analysis. The following metrics rely on the USV in question to produce a log file of the format: "timestamp, latitude, longitude, UTMEasting, UTMNorthing, nextUTMEasting, nextUTMNorting". This log file will be used in the following subsections to describe how time, distance, percent coverage, root mean squared cross-tracked error, and Hausdorff distance can be measured and calculated.

3.3.1 Survey Time

The survey is defined to begin when the vehicle reaches the first waypoint to traverse to, and the survey ends when the vehicle reaches the last waypoint to traverse to. This allows traversing to and from the home base to not affect the final results.

3.3.2 Path Length

As described earlier, a log file with "timestamp, latitude, longitude, UTMEasting, UTMNorthing, nextUTMEasting, nextUTMNorting" is needed to compute path length. The path length can be calculated easily by using the distance formula as seen below:

$$distance = \sqrt{(x_2 - x_1)^2 + (y_2 - y_1)^2}$$

For example, let the array log contain a list of n many (UTMEasting, UTMNorthing) coordinates. The below code will calculate the total distance of the survey in meters:

```
double totalDistance = 0.0;
for (int loopC = 0; c < n-1; c++)
{
   totalDistance += distance(log[n],log[n+1]);
}
```

3.3.3 RMS Cross-track Error and Hausdorff Distance

Cross-track error is the distance the boat is from the desired path in meters. With a log file of the form: "timestamp, latitude, longitude, UTMEasting, UTMNorthing, nextUTMEasting, nextUTMNorting", calculating the cross-track error can be calculated by finding the distance from the point (UTMEasting, UTMNorthing) to the intended line segment with endPoints (nextUTMEasting, nextUTMNorting) and the waypoint most recently visited. The root mean square is defined as the square root of the arithmetic mean of the squares of a set of numbers. Once all cross-track errors had been calculated, the root mean square is taken for all errors calculated during the time of the survey. In order to calculate the Hausdorff Distance, the maximum of the set of all cross-track errors is returned.

3.3.4 Percent Coverage

The typical coverage problem as seen in the literature states that the intended goal of the robot is to pass over each point in the environment. This situation applies to de-mining [1], lawn mowing [2], and painting [3], to name a few. This is not the case in this thesis since the robot is not carrying an implement that must touch every point in the space. The payload the USV will carry is an UltraRadiac radiation detector. This sensor is omni-directional in that the sensor does not have to be pointing in a particular orientation to make a reading. With this said, a sensor reading at a given (latitude,longitude) represents a reading for the circular area with center (latitude, longitude) and radius $transectSpacing/2$. The radius is defined as $transectSpacing/2$ since each straight portion of the generated path will run parallel to another straight portion $transectSpacing$ units to the right and left. The problem of calculating percent coverage then breaks down into calculating the area of n many circles. This problem has been looked into since at least 1978 when

Kratky published work in Journal of Physics A: Mathematical and General [14]. Due to this thesis focusing on the path plan performance, a percent coverage area approximation algorithm was written in Matlab. The area approximation algorithm uses the Monte-Carlo approach in which a bounding area is formed outside the circles (the original bounding area of the survey). Random points are then generated inside the area then checked to see if the random point falls inside any of the circles or not. The steps for this algorithm are as follows:

1. Calculate the centroid of the bounding polygon.
2. Divide the bounding polygon into triangles with each triangle sharing a similar vertex, the centroid.
3. Calculate the area of each triangle.
4. Use the area of all triangles as a PDF so a random number is generated corresponding to a uniform random triangle.
5. Generate a random point in the random triangle from Step 4.
6. Using the distance formula, determine if the random point lies within any of the circles formed from the collected data.
7. If the random point is inside at least one of the circles, mark a hit, else mark a miss. If in more than 1 circle, this does not matter.
8. Repeat steps 4-7 n many times (n greater than or equal to 100,000).
9. Percent covered is then calculated as the number of hits divided by the number of total random points generated.

10. Area of coverage is equal to percent covered times the area of the bounding polygon, or the sum of the areas of all its inscribed triangles.

The below figure shows the output of this area approximation algorithm from data collected on May 12, 2015, at Disaster City by the Challenge 1. The resulting survey resulted in 54.14% coverage. The area in blue denotes the area that was surveyed and the area in red is area that was not surveyed. This particular run was completed with an incorrect path plan resulting in the Challenge 1 USV not completing transects towards the center of the polygon. This accounts for the larger area of red in the center of the polygon. With the correct implementation of a lawn mower and the new spiral-like path plan, this thesis explores the area that is not surveyed between transects as well as locations outside of the intended bounding polygon.

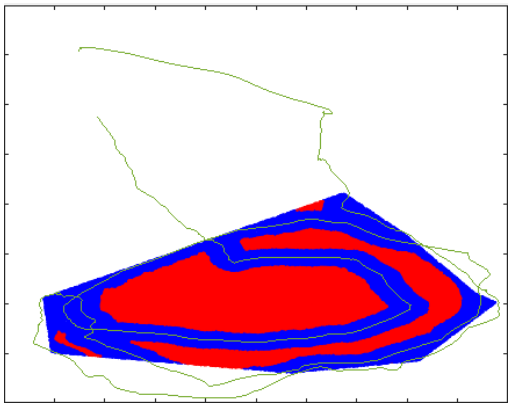

Figure 3.4: An example of percent coverage calculated from preliminary data.

NOTE: to remove factors introduced by a possible sampling inconsistency by the onboard radiation payload, the location of the boat taken once every second will be used to calculate percent coverage. The onboard radiation payload will occasionally

read in noise resulting in a corrupt reading to be written to the log file as well. The payload has also been seen to give readings in 1 to 3 second intervals, rather than exactly once every second. Since this thesis is primarily focusing on the path plan used (raster vs. spiral-like), it would not be right to penalize a certain path plan for an error with the payload.

3.3.5 Percentage of Locations Inside Boundary

Percentage of location inside the boundary was a post experiment metric that was added to help explain why a certain path plan resulted in lower than anticipated percent coverage. Percentage of locations inside the boundary is defined as number of locations inside the boundary divided by the total number of locations making up said survey. A traditional approach for determining if a point is inside a simple, non-intersecting polygon is the Winding Number method. The Winding Number method counts the number of times the polygon winds around the point P. The point is outside the polygon if and only if the Winding Number is equal to zero, other wise the point is inside the polygon. The below code was used to determine if each GPS location is inside the bounding area or not. As stated above, if a call to wnPnPoly returns a value of zero, the point is not in the polygon. If a value other than zero is returned, the point is inside the polygon.

```
public static double isLeft(Point P0,Point P1,Point P2)
{
   return((P1.x-P0.x)*(P2.y-P0.y)-(P2.x-P0.x)*(P1.y-P0.y));
}

public static int wnPnPoly(Point P,ArrayList<Point>
   boundary)
{
   int   wn = 0;       // the winding number counter
   int n=boundary.size()-1; //number of vertices of
      boundary
```

```
    // loop through all edges of the polygon
    for(int i=0;i<n;i++)
    {
       // edge from V[i] to V[i+1]
       if (boundary.get(i).y <= P.y)
       {  // start y <= P.y
          if(boundary.get(i+1).y>P.y)
          {
              // an upward crossing
              if(isLeft(boundary.get(i),
                 boundary.get(i+1),P)>0)
              {
                 // P left of edge
                 ++wn; // have a valid up intersect
              }
          }
       }
       else
       {
          // start y > P.y (no test needed)
          if (boundary.get(i+1).y <= P.y)
          {
             // a downward crossing
             if(isLeft(boundary.get(i),boundary.get(i+1),P)<0)
             {
                // P right of edge
                --wn; // have a valid down intersect
             }
          }
       }
    }
    return wn;
}
```

4. IMPLEMENTATION

The following chapter explains how the approach from Chapter 3 was implemented on the Challenge 1 System. All software written was developed using Java with the Netbeans text editor. It is important to note, that all these changes are on the offboard, operator control laptop. This means that no changes were made to the Lutra 1.1's onboard software controller.

4.1 Spiral-like Path Plan

The spiral-like algorithm described in the previous chapter was created due to the original spiral-like algorithm presented in [28] inability to maintain parallel transects. As can be seen in Figure 4.1, the old version of the spiral-like algorithm (yellow path) does not have consistent, much less parallel transects. For example, the transect spacing on the right side of the figure is much more narrow than the transect spacing on portions on the top, bottom, or left side of the figure. It was also determined that the old version of the spiral path plan used the function `getOuterBoundary()`, a function that finds a smaller, conservative "safe" inner boundary. The problem with this, as will be seen later in the Raster section of this chapter, is that the resulting bounding area is not the user defined convex polygon, resulting in an incomplete coverage plan.

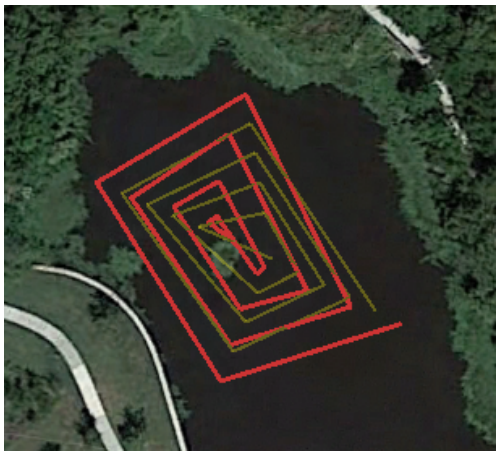

Figure 4.1: The yellow path indicates the the original spiral-like algorithm presented in [28]. The red path is the newly created, spiral-like algorithm.

4.2 Raster Scan Path Plan

The Lutra Airboat 1.1 is originally equipped with an explore area functionality. After the user selects the bounded area to survey in the Operator Interaction Window, a raster scan path plan is generated and the resulting list of waypoints to traverse to is sent to the boat. The original raster scan was seen to have two problems. First, the raster scan did not allow generated waypoints to be extended out to the intended user's bounding area. Instead, all generated points were well within the bounding area which therefore resulted in an incomplete coverage of the area. Second, this path plan does not account for wind direction though, but instead has the vehicle traveling east to west and west to east. As is common practice for fixed-winged aircraft, the vehicle in question is manoeuvered to fly with and against the wind (parallel to the wind direction), and the vehicle does not fly with a cross wind (perpendicular to the wind direction). In Figure 4.2, one can see that the original raster scan the Lutra 1.1 came with (red path) does not orient with the wind as well as does not extend to the bounding convex polygon. It was determined that

the old version of the raster path plan used the function `getOuterBoundary()`, a function that finds a smaller, conservative "safe" inner boundary. This is why the red path in Figure 4.2 did not extend out to the user defined bounding area.

Figure 4.2: The red path indicates the Lutra 1.1's original raster scan. The yellow path is the newly created, wind-oriented raster scan.

With this said, the original raster scan the Lutra Airboat 1.1 came equipped has been completely re-written so that intended waypoints are extended to the bounding edges as well as the implementation of a user defined parameter *wind heading (wh)* that is used to orient the transects of the path plan parallel to the wind direction. Refer the previous chapter for the specifics of this algorithm. The below table has the wind directions and their associated wind parameter.

Wind Direction	Parameter
East, West	0
East South East, West North West	22.5
South East, North West	45
South South East, North North West	67.5
North, South	90
North North East, South South West	112.5
North East, South West	135
East North East, West South West	157.5

Table 4.1: Wind parameters

5. EXPERIMENTS AND RESULTS

In this section, the author describes the experiment conducted to evaluate the overall system and analyze the difference between the newly created spiral-like path plan, and the wind-oriented raster scan.

5.1 Hypotheses

The following hypothesis will be considered:

1. When compared to a wind-oriented raster scan, the spiral-like path plan will result in the shortest survey time carried out by the robot.
2. When compared to a wind-oriented raster scan, the spiral-like path plan will result in the shortest path length carried out by the robot.
3. When compared to a wind-oriented raster scan, the spiral-like path plan will result in a lower RMS of cross-track error.
4. When compared to a wind-oriented raster scan, the spiral-like path plan will result in a lower Hausdorff Distance.
5. When compared to a wind-oriented raster scan, the spiral-like path plan will result in a greater percentage of coverage.

The sixth measure, percentage of locations located inside the bounding area, was a post test measure that was added to further understand why a particular path plan resulted in the percent coverage that it did.

5.2 Experimental Method

To test these hypothesis, the author used the pond at John Crompton Park in College Station, Texas. 25 different convex polygons with the number of vertices

ranging from four to seven were created via teleoperation of the Challenge 1 USV. A map of the park can be found below (Figure 5.1). According to the City of College Station website, John Crompton Park has a fishing pond of approximately 1.15 acres [20]. Twenty-five different polygons was chosen as the maximum due to each run having an expected average time of thirty minutes. Fifty runs multiplied by thirty minutes is the equivalent of twenty-five hours. Assuming five complete pairs can be calculated per day (ten total runs), this would result in five complete days of trials needed.

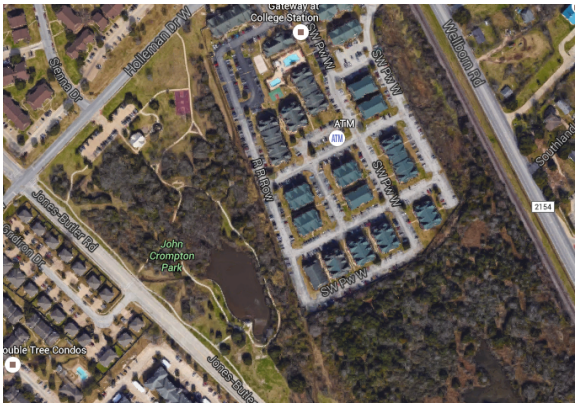

Figure 5.1: A Google Earth image of John Crompton Park in College Station, Texas.

For each convex polygon, the Challenge 1 surveyed the area (water) two times using the following path configuration order: Spiral then Raster Scan or, Raster Scan then Spiral. A transect spacing of .00004 degrees (or approximately 4.45 m) was used for both the raster scan and spiral path plan. Degrees were used instead of meters since the original raster scan the Lutra 1.1 came equipped with was written using degrees. This spacing was chosen because it allowed for test trials conducted at John Crompton park to last between 5-30 minutes. If either the spiral or raster scan failed,

all data collected for that given polygon were discarded. In other words, a successful trial was entered into the final data if and only if both the spiral and raster scans are successfully completed one after the other. Failure in a trial was constituted as the boat getting stuck and requiring operator assistance to free, termination of path traversal before all waypoints are traversed to, or a trial that exceeds the thirty minute time limit. The operator was notified that all waypoints have been traversed to once the intended path disappears from the OCU as well as the onboard motor turning off. The alternating path plans allow each polygon to be surveyed with each path and allows weather to affect the different path plans in a similar fashion. In total, fifty runs of experimentation were conducted, resulting in twenty-five pairs. The trials took place over multiple days. In order to reduce a bias from affecting the trials, the daily order was randomized. The below table has the path plan order for all five days in which trials were completed.

Day Number	Path Plan Order
1	Spiral, Raster
2	Spiral, Raster
3	Raster, Spiral
4	Raster, Spiral
5	Spiral, Raster

Table 5.1: Experimental path order

Prior to the beginning of each run and after the completion of each run, the wind direction and speed were recorded. Wind speed was measured using a Ambient

Weather WM-2 Handheld Weather Meter. The wind direction was noted from the The Weather Channel IPhone application, and was verified using the wind meter and compass on said IPhone. Prior to each run, this documented direction was entered as a parameter to the Operator Control Unit so that the raster scan could be oriented with and against the wind.

Below in Figure 5.2 an example of a path plan comparison trial is presented. The yellow line indicates the intended oriented raster scan oriented with a North North West wind (67.5 degrees). The red line indicates the spiral path plan for the same bounded region. The spiral path plan is not dependent on the wind direction in any way.

Figure 5.2: Path plan comparison between an oriented raster scan (yellow line) and a spiral like path plan (red line)

Below in Figure 5.3 and Figure 5.4 are the two actual paths carried out by the Challenge 1 during Trial 1. Both images are visual proof that neither of the path plans performed exactly as intended. For example in both Figures 5.3 and 5.4, it

can be seen that the transect spacing is not consistent throughout, path segments are not straight, and there is overlap present.

Figure 5.3: Trial 1 raster path

Figure 5.4: Trial 1 spiral path

5.3 Data Recorded

Following the completion of the twenty-five pairs (fifty runs), the log files generated from the run were used to calculate total survey time, total survey distance,

RMS cross-track error, maximum track error (also known as Hausdorff Distance), percent coverage, and percentage of points inside the boundary. For each metric, an associated results section is presented. Wind parameters used in all 25 trials (50 runs) can be found in Appendix 1.

5.3.1 Total Survey Time

Total survey time was calculated by subtracting the time at which the Challenge 1 reached its first waypoint from the time that the Challenge 1 reached its last waypoint. This eliminated the time the Challenge 1 used to traverse to and from the operator's home base. The below table shows all the calculated times as well as the differences between the two times. A positive difference indicates that the raster path plan took longer to execute and a negative difference indicates that the spiral path took longer to execute.

Trial Number	Raster Survey Time (seconds)	Spiral Survey Time (seconds)	Difference (seconds)
1	508	519	-11
2	601	586	15
3	636	642	-6
4	448	250	198
5	669	573	96
6	505	436	69
7	458	462	-4
8	452	362	90
9	488	493	-5
10	509	472	37
11	471	492	-21
12	427	303	124
13	495	477	18
14	638	938	-300
15	669	573	96
16	448	510	-62
17	586	636	-50
18	533	636	-103
19	536	694	-158
20	672	762	-90
21	686	536	150
22	611	663	-52
23	929	1058	-129
24	1069	810	259
25	701	520	181

Table 5.2: The survey times for each path plan (Raster and Spiral) for all 25 trials. A positive difference indicates the Spiral executed in a shorter period of time. A negative difference indicates the Raster executed in a shorter period of time.

5.3.2 Total Survey Distance

Total survey distance was calculated by determining the distance in meters between each of the records in the associated log file. The Challenge 1's source code logs the current position of the the vehicle in both latitude,longitude as well as in UTM Coordinates for each record that is taken once per second. The GPS used by the Challenge 1 is the GPS used by the Nexus 4 smartphone. The Nexus 4 used an Avago 3012 GPS chip, leading to 3 to 4 meter accuracy. Similar to survey time, records were only used towards the calculation overall survey distance if the timestamp of the record was between the interval of the start time and end time. This eliminated the distance the Challenge 1 traversed to and from the home base prior to and after the completion of the survey. The below table shows all the calculated total survey distances as well as the difference between the two distances. A positive difference indicates that thee raster path plan had a larger survey distance and a negative difference indicates the spiral path had a larger survey distance.

Trial	Distance Raster (meters)	Distance Spiral (meters)	Difference (meters)
1	288.54	278.59	9.95
2	307.76	305.94	1.82
3	283.84	311.92	-28.07
4	238.29	165.94	72.35
5	274.55	264.31	10.24
6	241.59	240.33	1.26
7	263.84	282.95	-19.11
8	254.89	228.11	26.78
9	248.30	232.09	16.21
10	242.70	298.33	-55.63
11	224.94	241.88	-16.94
12	164.84	163.43	1.41
13	264.30	256.15	8.15
14	337.92	414.17	-76.24
15	274.55	264.31	10.24
16	209.77	242.50	-32.73
17	273.08	335.85	-62.77
18	224.36	297.75	-73.39
19	247.91	297.88	-49.98
20	288.08	348.54	-60.46
21	239.84	257.15	-17.31
22	192.49	254.73	-62.24
23	329.95	385.32	-55.36
24	381.20	328.18	53.02
25	226.56	215.91	10.65

Table 5.3: The total distance for each path plan (raster and spiral) for all 25 trials. A positive difference indicates the spiral had a lower total distance. A negative difference indicates the raster had a lower total distance.

5.3.3 RMS Cross-Track Error

Root Mean Cross-Track Error was calculated by determining the distance in meters between the Challenge 1's current location to the line segment who's endpoints are the vehicle's last waypoint visited and the waypoint the vehicle is currently traversing to. Similar to survey distance, records from the log file were only used towards the calculation of RMS Cross-Track Error if the timestamp of the record was between the interval of the start time and end time. This eliminated the cross-track error incurred by the Challenge 1 as it traversed to and from the home base prior to and after the completion of the survey. The below table shows all the calculated RMS Cross-Track Error as well as the difference between the two values. A positive difference indicates that thee raster path plan had a larger RMS Cross-Track Error and a negative difference indicates the spiral path had a larger RMS Cross-Track Error.

Trial Number	Raster RMS (meters)	Spiral RMS (meters)	Difference (meters)
1	2.16	2.17	-0.01
2	2.63	2.80	-0.18
3	3.22	2.83	0.39
4	2.66	1.40	1.26
5	2.85	2.87	-0.02
6	4.06	2.10	1.96
7	3.24	2.47	0.77
8	3.16	2.75	0.42
9	2.31	3.26	-0.95
10	2.28	1.99	0.29
11	2.40	3.00	-0.61
12	2.62	2.08	0.55
13	3.08	2.43	0.65
14	2.57	2.59	-0.03
15	2.85	2.87	-0.02
16	3.01	2.83	0.18
17	2.81	3.63	-0.82
18	2.99	4.77	-1.78
19	3.09	3.43	-0.34
20	2.91	2.60	0.31
21	4.99	2.06	2.93
22	4.82	3.87	0.95
23	3.58	3.87	-0.29
24	4.43	3.07	1.36
25	3.81	3.11	0.70

Table 5.4: The RMS for each path plan (raster and spiral) for all 25 trials. A positive difference indicates the spiral had a lower RMS. A negative difference indicates the raster had a lower RMS.

5.3.4 Hausdorff Distance (Max Cross-track Error)

Hausdorff Distance was calculated by determining the maximum distance in meters between the Challenge 1's current location to the line segment who's endpoints are the vehicle's last waypoint visited and the waypoint the vehicle is currently traversing to. Similar to RMS Cross-Track Errror, records from the log file were only used towards the calculation of Hausdorff if the timestamp of the record was between the interval of the start time and end time. This eliminated the Hausdorff Distance incurred by the Challenge 1 as it traversed to and from the home base prior to and after the completion of the survey. The below table shows all the calculated Hausdorff Distance as well as the difference between the two values. A positive difference indicates that thee raster path plan had a larger Hausdorff Distance and a negative difference indicates the spiral path had a larger Hausdorff Distance.

Trial	Hausdorff Distance Raster (meters)	Hausdorff Distance Spiral (meters)	Difference (meters)
1	7.07	4.21	2.86
2	6.77	5.75	1.02
3	6.78	6.08	0.7
4	6.38	3.44	2.94
5	8.06	7.81	0.25
6	10.77	4.33	6.44
7	11.05	5.19	5.86
8	8	4.92	3.08
9	8.06	5.01	3.05
10	7.62	5.83	1.78
11	5.97	6.71	-0.73
12	7.25	5.58	1.67
13	6.85	7	-0.15
14	7.07	6.14	0.93
15	8.06	7.81	0.25
16	6.71	6.17	0.54
17	6.96	7.13	-0.17
18	7.21	8.63	-1.42
19	8.06	7.6	0.46
20	6.99	5	1.99
21	8.33	6.32	2
22	9.95	7.28	2.67
23	8.7	8	0.7
24	8.44	6.96	1.48
25	6.4	6.52	-0.11

Table 5.5: The Hausdorff distance for each path plan (Raster and Spiral) for all 25 trials. A positive difference indicates the spiral had a lower Hausdorff distance. A negative difference indicates the raster had a lower Hausdorff distance.

5.3.5 Percent Coverage

Percent Coverage was approximated using the Monte-Carlo method presented in the Section 3.3.4 of this thesis. To recap, each location (latitude and longitude) of the Challenge 1 throughout the mission represented a surveyed circular area who's center is at the latitude and longitude of the vehicle with radius $.5 * transectSpacing$. This lead to a set of circles S, with each element c being a circle with the components (latitude,longitude,radius). To approximate the area, first 100,000 random points were generated inside the user defined convex polygon. Then, each of the 100,000 points was tested to see if it was inside at least one of the circles c in set S. If the random point was inside at least one of the circles in S, a counter for total hits was incremented, else a counter for total misses was incremented. Following the testing of all 100,000 random points, percent coverage was calculated by taking the total number of hits and dividing it by 100,000. As for all previous metrics of this thesis, only locations between the interval (startTime, endTime) were considered as to eliminate any coverage that would have been incurred traversing to and from the home base. The below table shows all the calculated percent coverages for each of the 50 total trials as well as the differences between the two percentages. A positive difference indicates the spiral path plan resulted in a higher percent coverage and a negative difference indicates the spiral path plan had a higher percent coverage.

Trial	Coverage Raster	Coverage Spiral	Difference
1	0.83	0.85	-0.03
2	0.71	0.73	-0.01
3	0.81	0.77	0.05
4	0.87	0.74	0.13
5	0.68	0.69	-0.01
6	0.73	0.76	-0.03
7	0.73	0.65	0.07
8	0.80	0.85	-0.05
9	0.73	0.71	0.02
10	0.73	0.76	-0.04
11	0.73	0.62	0.11
12	0.70	0.60	0.10
13	0.82	0.78	0.03
14	0.72	0.82	-0.09
15	0.68	0.69	-0.01
16	0.64	0.67	-0.02
17	0.72	0.61	0.11
18	0.76	0.47	0.29
19	0.78	0.70	0.08
20	0.72	0.69	0.03
21	0.75	0.79	-0.04
22	0.83	0.66	0.16
23	0.76	0.71	0.05
24	0.65	0.69	-0.05
25	0.79	0.60	0.19

Table 5.6: The percent coverage for each path plan (raster and spiral) for all 25 trials. A positive difference indicates the raster had a higher percent coverage. A negative difference indicates the spiral had a higher percent coverage.

5.3.6 Percent of Locations in the Bounding Area

Percentage of locations in the bounding area was a post experiment metric added to help explain why the percent coverage for the spiral path plan was lower than originally anticipated. Percentage of location in the bounding area was determined by using the Winding Number method that was presented in Section 3.3.5. To determine the total percentage of locations in the bounding area, the total number of locations in the bounding area was divided by the total number of locations throughout the survey, or in the interval of (startTime, endTime). The below table shows all the percentage of locations inside the bounding area as well as the differences between the two percentages. A negative difference indicates the spiral path plan had a higher percentage of locations in the bounding area, and a positive difference indicates the raster scan had a higher percentage of locations in the bounding area.

Trial Number	Percent In Raster	Percent In Spiral	Difference
1	0.96	1.00	-0.04
2	0.89	0.84	0.05
3	0.87	0.65	0.22
4	0.95	0.89	0.06
5	0.79	0.71	0.08
6	0.71	0.65	0.07
7	0.93	0.52	0.41
8	0.96	1.00	-0.04
9	0.87	0.99	-0.12
10	0.98	0.66	0.33
11	0.78	0.44	0.34
12	0.88	0.50	0.38
13	0.72	0.86	-0.15
14	0.88	0.64	0.23
15	0.79	0.71	0.08
16	0.80	0.54	0.26
17	0.83	0.44	0.38
18	0.87	0.24	0.63
19	0.87	0.51	0.35
20	0.80	0.67	0.12
21	0.49	0.64	-0.15
22	0.68	0.45	0.23
23	0.73	0.56	0.17
24	0.61	0.54	0.07
25	0.71	0.46	0.26

Table 5.7: The percent of locations in the bounding area for each path plan (raster and spiral) for all 25 trials. A positive difference indicates the raster had a higher percent of locations in the bounding area. A negative difference indicates the spiral had a higher percent of locations in the bounding area.

5.4 Results

The remainder of this chapter presents a subsection for each of the six measured and calculated metrics. In each subsection, the statistical results for each metric are given as well as the results for each of the associated hypothesis.

5.4.1 Total Survey Time Results

Following the completion of all total survey time calculations, the average survey time, standard error, and confidence intervals for each of the two executed path plans was found. As can be seen in Table 5.8, the population average survey time for the spiral scan was 13.68 seconds shorter than that of the population average total survey time of the raster scan. A statistical two-tailed, paired t-test was conducted, to determine if the population average survey time would always be be less for a spiral path plan versus a raster can. The results of this test are presented in Table 5.9.

	Raster	Spiral
Average Survey Time	589.80	576.12
Standard Error	30.37	36.33
95% Confidence	(527.10, 652.49)	(501.13, 651.10)

Table 5.8: Summary of results - average survey time for both raster and spiral Path plans. All values are in seconds.

Below are the two hypothesis that are considered in this portion. Hypothesis 1 is the null hypothesis that assumes that the difference between the population mean is equal to zero. Alternatively, Hypothesis 1a assumes the population mean of survey time is not equal to zero.

Hypothesis 1 $\mu_{diffSurveyTime} = 0$

Hypothesis 1a $\mu_{diffSurveyTime} \neq 0$

	Raster and Spiral
df	24
t-stat	0.554299526
t-critical (two tail)	2.063898547
p-value	0.584502563
95% Confidence Interval	(-37.25,64.61)

Table 5.9: Summary of t-test - average survey time in raster and spiral

As the results of Table 5.9 show, a p-value of .58 was found. Since this value is not less than $\alpha = .05$, this leads to a failure to reject the null hypothesis. This means there is not enough evidence available to suggest the null hypothesis is false at the 95% confidence level. In conclusion, it can be determined that for these twenty-five trials, neither the raster scan or spiral path plan resulted in statically shorter survey times.

5.4.2 Total Survey Distance Results

Following the completion of all total survey distance calculations, the averages survey distance, standard error, and confidence intervals for each of the two executed path plans was found. As can be seen in Table 5.10, the average population survey distance for the raster scan was 15.53 meters less than that of the population average of total survey distance of the spiral path. A statistical two-tailed, paired t-test was

conducted to determine if the population average of total survey distance for the raster scan path plan would always be less than that of the population mean of the total survey distance for a spiral path plan. The results of this test are presented in Table 5.11.

	Raster	Spiral
Average Survey Distance	260.96	276.49
Standard Error	46.67	59.14
95% Confidence	(241.69, 280.23)	(252.07 ,300.90)

Table 5.10: Summary of results - average total survey distance for both raster and spiral path plans. All values are in meters.

Below are the two hypothesis that are considered in this portion. Hypothesis 2 is the null hypothesis that assumes that the difference between the population mean of survey distance is equal to zero. Alternatively, Hypothesis 2a assumes the population mean of survey distance is not equal to zero.

Hypothesis 2 $\mu_{diffSurveyDistance} = 0$

Hypothesis 2a $\mu_{diffSurveyDistance} \neq 0$

	Raster and Spiral
df	24
t-stat	-1.96051
t-critical (two tail)	2.063899
p-value	0.061643
95% Confidence Interval	(-31.87,0.81)

Table 5.11: Summary of t-test - average total distance in raster and spiral

As the results of Table 5.11 show, a p-value of .06 was found. Since this value is not less than $\alpha = .05$, this leads to a failure to reject the null hypothesis. This means there is not enough evidence available to suggest the null hypothesis is false at the 95% confidence level. In conclusion, it can be determined that for these twenty-five trials, neither the raster scan or spiral path plan resulted in statically shorter survey distances.

5.4.3 RMS of Cross-Track Error Results

Following the completion of all total RMS of Cross-Track Error calculations, the averages of RMS of Cross-Track Error, standard error, and confidence intervals for each of the two executed path plans was found. As can be seen in Table 5.12, the population average of RMS of Cross-Track Error for the spiral-like was .31 meters less than that of the population average of RMS of Cross-Track Error of the raster-scan. A statistical two-tailed, paired t-test was conducted to determine if the population average of RMS of Cross-Track Error for the spiral-like path plan would always be less than that of the population average of the RMS Cross-Track Error for a raster scan. The results of this test are presented in Table 5.13.

	Raster	Spiral
Average RMS	3.14	2.83
Standard Error	0.15	0.14
95% Confidence	(2.82, 3.45)	(2.53, 3.13)

Table 5.12: Summary of results - average RMS for both raster and spiral path plans. All values are in meters.

Below are the two hypothesis that are considered in this portion. Hypothesis 3 is the null hypothesis that assumes that the difference between the population mean of RMS Cross-Track Error is equal to zero. Alternatively, Hypothesis 3a assumes the population mean of RMS Cross-Track Error is not equal to zero.

Hypothesis 3 $\mu_{diffRMSCrossTrackError} = 0$

Hypothesis 3a $\mu_{diffRMSCrossTrackError} \neq 0$

	Raster and Spiral
df	24
t-stat	1.599085
t-critical (two tail)	2.063899
p-value	0.122885
95% Confidence Interval	(-0.08,0.70)

Table 5.13: Summary of t-test - average RMS in raster and spiral

As the results of Table 5.13 show, a p-value of .122885 was found. Since this value is not less than $\alpha = .05$, this leads to a failure to reject the null hypothesis. This means there is not enough evidence available to suggest the null hypothesis is false at the 95% confidence level. In conclusion, it can be determined that for these twenty-five trials, neither the raster scan or spiral path plan resulted in statically smaller RMS Cross-Track Error.

5.4.4 Hausdorff Distance Results

Following the completion of all total Hausdorff Distance calculations, the averages of Hausdorff Distances, standard error, and confidence intervals for each of the two executed path plans was found. As can be seen in Table 5.14, the population average of Hausdorff Distance for the spiral path plan was 1.53 meters less than that of the population average of Hausdorff Distance of the raster scan. A statistical two-tailed, paired t-test was conducted to determine if the population average of Hausdorff Distance for the spiral path plan would always be less than that of the population average of the Hausdorff Distance of the rastor scan. The results of this test are presented in Table 5.15.

	Raster	Spiral
Average Hausdorff Distance	7.74	6.21
Standard Error	0.25	0.26
95% Confidence	(7.20, 8.27)	(5.67, 6.75)

Table 5.14: Summary of results - Hausdorff distance for both raster and spiral path plans. All values are in meters.

Below are the two hypothesis that are considered in this portion. Hypothesis 4 is the null hypothesis that assumes that the difference between the population mean of Hausdorff Distance is equal to zero. Alternatively, Hypothesis 3a assumes the population mean of Hausdorff Distance is not equal to zero.

Hypothesis 4 $\mu_{diffHausdorffDistance} = 0$

Hypothesis 4a $\mu_{diffHausdorffDistance} \neq 0$

	Raster and Spiral
df	24
t-stat	4.103231
t-critical (two tail)	2.063899
p-value	0.000406
95% Confidence Interval	(0.75,2.28)

Table 5.15: Summary of t-test - average Hausdorff distance in raster and spiral

As the results of Table 5.15 show, a p-value of 0.000406 was found. Since this value is less than $\alpha = .05$, this leads to a rejection of the null hypothesis and an acceptance of the alternative hypothesis. This means there is enough evidence available to suggest the null hypothesis is false at the 95% confidence level. In conclusion, it can be determined that for these twenty-five trials, the spiral path plan will result in a statistically significant lower population average for Hausdorff Distance. The confidence interval presented in Table 5.15 shows that one can be 95% sure that the true mean decrease in Hausdorff Distance from that of the raster scan to a spiral path plan lies between 0.75 meters and 2.28 meters.

5.4.5 Percent Coverage Results

Following the completion of all total Percent Coverage calculations, the averages of Percent Coverages, standard error, and confidence intervals for each of the two executed path plans was found. As can be seen in Table 5.16, the population average of Percent Coverage for the raster scan path plan was 4.22% percent more than that of the population average of Percent Coverage of spiral scan. A statistical two-tailed, paired t-test was conducted to determine if the population average of Percent Coverage for the raster scan path plan would always be more than that of the population average of the Percent Coverage of the spiral path plan. The results of this test are presented in Table 5.17.

	Raster	Spiral
Average Percent Coverage	0.7469	0.7047
Standard Error	0.0113	0.0173
95% Confidence	(0.72, 0.77)	(0.66, 0.74)

Table 5.16: Summary of results - average percent coverage for both raster and spiral path plans.

Below are the two hypothesis that are considered in this portion. Hypothesis 5 is the null hypothesis that assumes that the difference between the population mean of Percent Coverage is equal to zero. Alternatively, Hypothesis 5a assumes the population mean of Percent Coverage is not equal to zero.

Hypothesis 5 $\mu_{diffPercentCoverage} = 0$

Hypothesis 5a $\mu_{diffPercentCoverage} \neq 0$

	Raster and Spiral
df	24
t-stat	2.368744
t-critical (two tail)	2.063899
p-value	0.026241
95% Confidence Interval	(0.0054,0.0791)

Table 5.17: Summary of t-test - average percent coverage in raster and spiral

As the results of Table 5.17 show, a p-value of 0.026241 was found. Since this value is less than $\alpha = .05$, this leads to a rejection of the null hypothesis and an acceptance of the alternative hypothesis. This means there is enough evidence available to suggest the null hypothesis is false at the 95% confidence level. In conclusion, it can be determined that for these twenty-five trials, the raster scan path plan will result in a statistically significant higher population average for Percent Coverage. The confidence interval presented in Table 5.17 shows that one can be 95% sure that the true mean increase in Percent Coverage from that of the spiral path plan to a raster scan path plan lies between 0.54% and 7.91%.

5.4.6 Percentage of Locations In the Bounding Area Results

Following the completion of all total percentage of locations in the bounding area, the averages of percentage of locations in the bounding area, standard error, and confidence intervals for each of the two executed path plans was found. As can be seen in Table 5.18, the population average of percentage of locations in the bounding area for the raster scan path plan was 16.88% percent more than that of the population average of Percent Coverage of spiral scan. A statistical two-tailed,

paired t-test was conducted to determine if the population average of percentage of locations in the bounding area for the raster scan path plan would always be more than that of the population average of the percentage of locations in the bounding area of the spiral path plan. The results of this test are presented in Table 5.19.

	Raster	Spiral
Average Percent Locations in the Bounding Area	0.8138	0.6450
Standard Error	0.1179	0.1965
95% Confidence	(0.7651, 0.8624)	(0.5638, 0.7261)

Table 5.18: Summary of results - average percent of locations in the bounding area for both raster and spiral path plans.

Below are the two hypothesis that are considered in this portion. Hypothesis 6 is the null hypothesis that assumes that the difference between the population mean of percentage of locations in bounding area is equal to zero. Alternatively, Hypothesis 6a assumes the population mean of percentage of locations in bounding area is not equal to zero.

Hypothesis 6 $\mu_{diffPercentInBoundingArea} = 0$

Hypothesis 6a $\mu_{diffPercentInBoundingArea} \neq 0$

	Raster and Spiral
df	24
t-stat	4.332591
t-critical (two tail)	2.063899
p-value	0.000227
95% Confidence Interval	(0.0883,0.2492)

Table 5.19: Summary of t-test - average percent of locations in the bounding area in raster and spiral

As the results of Table 5.19 show, a p-value of .000227 was found. Since this value is less than $\alpha = .05$, this leads to a rejection of the null hypothesis and an acceptance of the alternative hypothesis. This means there is enough evidence available to suggest the null hypothesis is false at the 95% confidence level. In conclusion, it can be determined that for these twenty-five trials, the raster scan path plan will result in a statistically significant higher population average for percentage of locations in the bounding area. The confidence interval presented in Table 5.17 shows that one can be 95% sure that the true mean increase in percentage of locations in the bounding area from that of the spiral path plan to a raster scan path plan lies between 8.83% and 24.92%.

To further explain why the percent of locations in the bounding area was so low for the spiral scan, the above metric was modified for the spiral path plan so that the percentage of locations on the spiral's first outer loop could be found. This modification consisted of using the same approach used previously, but only using locations of the Challenge 1 that were associated with line segments forming the spiral's outer loop. All other locations were not considered here, nor did the locations add to the overall total used to find the final percentage for each path. Table **??** shows the results that were obtained.

Trial Number	Percentage of Locations in the Bounding Area of the Outer Loop
1	1.00
2	0.67
3	0.17
4	0.84
5	0.43
6	0.26
7	0.12
8	1.00
9	0.98
10	0.25
11	0.10
12	0.26
13	0.63
14	0.14
15	0.43
16	0.21
17	0.12
18	0.01
19	0.16
20	0.30
21	0.21
22	0.05
23	0.03
24	0.15
25	0.05

Table 5.20: Percentage of locations inside the bounding area from the spiral's outer loop.

Following the completion of all total percentage of locations in the bounding area for the spiral's outer loop only, the averages of percentage of locations in the bounding area for the outer loop, standard deviation, standard error, sample variance,and confidence interval for each of the spiral's path plans was calculated. The results are presented below.

Mean	0.3429
Standard Error	0.0639
Standard Deviation	0.3199
95% Confidence Level	(0.2108, 0.4749)

Table 5.21: Summary of results for percentage of locations in the bounding area for the spiral's outer loop only.

As Table 5.21 shows, on average, only 34.29% of the spiral's outer loop was in the bounding box. With this low of a percentage of locations inside the bounded area, this percentage helps pinpoint where the spiral path plan preformed poorly, which in turn lead to a poor percentage of coverage for the spiral path plan.

6. DISCUSSION

Following the completion of the data analysis and statistical tests, it was observed that even though the spiral path plan resulted in a statistically significant lower max track error (1.52 meter decrease, $p < .002$), the raster scan resulted in a statistically significant higher percent coverage (4.22% increase,$p < .027$) and a higher percent of locations inside the bounding polygon (16.88% increase, $p < .002$). Due to the spiral path plan's inability to maintain a position inside the user defined bounding area, a wind oriented raster scan is the best path plan to use when surveying a bounded convex polygon with the Challenge 1 USV because it will insure a higher percentage of coverage while maintaining the same level of control as the novel spiral-like path plan. Similar control of the Challenge 1 when conducting a radiological survey by either a raster scan or spiral path plan is verified by the fact that neither of the two plans resulted in statistically shorter survey times, statistically shorter survey distance, or statistically smaller RMS of cross-track error. The figure below gives a visual example from Trial 12 that shows the Challenge 1's inability to consistently maintain locations inside the user defined bounding area when following a spiral like path, especially on the outer loop of the survey. As Figure 6.1 depicts, the Challenge 1 had large portions of each of the four sides of the outer loop outside the bounding area.

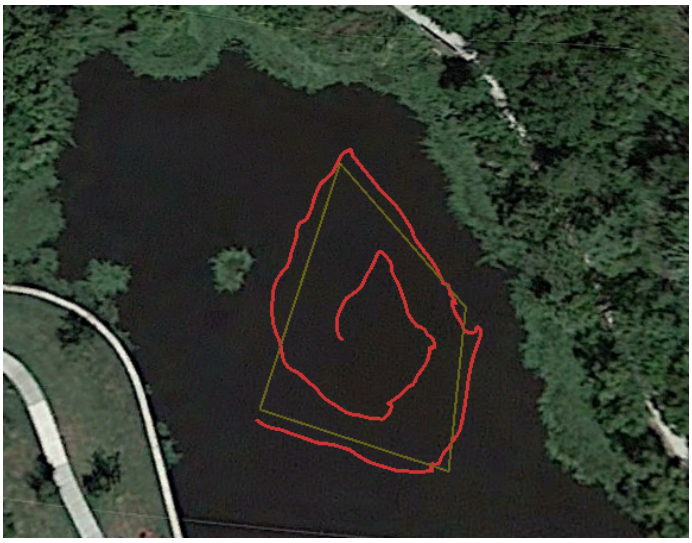

Figure 6.1: Trial 12 spiral path plan. The yellow polygon represents the user define bounding polygon. The red path indicates the path taken by the Challenge 1.

It can be concluded that the controller used for the Challenge 1 in this thesis is very poor, to say the least. This is evident in the fact that the average RMS of cross-track error for both the spiral-like path plan and the wind oriented raster scan was 2.83 m and 3.14 m respectively. For this thesis, the controller of this vehicle was not altered in any way from the original source code the Lutra 1.1 came equipped with. The PID parameters used for this thesis were set by a Platypus LLC employee. This employee visited Texas A&M University in the Spring of 2015 and set the parameters after testing conducted at Texas A&M's Research Park. These parameters were used since he was the employee that built and shipped the exact Lutra 1.1 used in this thesis. Due to the author's lack of knowledge regarding the control software running onboard the Lutra 1.1, the author did not want to risk compromising the Lutra 1.1. Therefore, only the software running offline on the operator's control laptop was altered.

As mentioned earlier, the Lutra 1.1 uses force vectoring to steer and move. To

recap, the Lutra 1.1 has a brushless motor with propeller mounted on a servo. In combination of the Lutra 1.1's on board control software and outputs from the onboard Arduino microcontroller, Pulse Width Modulation (PWM) was used to control the position of the mounted servo. In this thesis, the thrust of the brushless motor was never altered, in other words if the Lutra 1.1 was conducting a survey, the motor was on at a constant rate with the servo constantly altering its position. This lead to the Lutra 1.1 being able to make turns close to 180 degrees. This however is not the case for other types of surface vehicles such as the Emergency Integrated Lifesaving Lanyord or EMILY that uses force vectoring with a submerged jet pump or from all the other surface vehicles seen in the Literature Review of this thesis that used either duel underwater propellers or an in water rudder for steering.

In conclusion, for a USV such as the Lutra 1.1 and it's associated onboard controller, there was no significant difference between the RMS of cross-track error for either the spiral-like path plan or the wind oriented raster scan, but there was a significant difference in percent coverage. This means that for the Lutra 1.1 with wind speeds less than 7.7 mph (the max wind reading seen in this study) a wind-oriented raster scan should be used over a spiral-like path plan when conducting a radiological survey due to the spiral-like path plan's inability to maintain locations of the outer loop inside the user defined bounded polygon. This result is not guaranteed to hold for all unmanned surface vehicles. For example, a USV that is non-holonomic with a different steering mechanism and different controller could result in different outcomes than that of this thesis. The new leading candidate for implementation of the spiral path plan would be the EMILY. As mentioned in the related work section of this thesis, it is believed that this vehicle could have better control than that of the Challenge 1, which could lead to different results when comparing the raster scan to that of a spiral scan.

7. CONCLUSION AND FUTURE WORK

This chapter concludes the thesis with a recap of the overall study as well as presents the future work for this project.

7.1 Conclusion

The thesis describes the first known research into path planning used by small, unmanned surface vehicles for radiation detection and mapping. To begin, this thesis outlined the motivation for the creation of the Challenge 1 System by undergraduates participating in Texas A&M's AggiE Challenge. The Challenge 1 consists of three main components, the first being the Lutra 1.1 surface vehicle and onboard radiation sensing payload, second the path planning algorithms used to achieve an autonomous survey, and the third and final component being the off-line, post survey interpolation and heat map creation process. Following the Challenge 1's initial test with a cesium-137 radiological source at Texas A&M Engineering Extension Service's Disaster City® in College Station, Texas, the question of *Is a novel, spiral-like path plan better than a raster scan for a USV when conducting a survey of a bounded, obstacle free polygon?* was brought to the creators' attention. In order to quantitatively answer this question, a literature search was conducted in order to determine performance measures that could be used to help answer the main, overall question.

The literature review suggested that five performance metrics should be calculated following the Challenge 1's survey, those being: 1) Survey time, 2) Survey Distance, 3) Root Mean Square of Cross-track Error, 4) Hausdorff Distance (aka Max Cross-track Error), 5) Percent Coverage. To test the original hypothesis that a spiral scan would result in shorter survey times, shorter survey distances, smaller RMS of Cross-track Error, smaller Hausdorff Distances, and higher Percentage of

Coverage, 25 paired trials consisting of unique convex polygons, resulting in 50 total runs, were carried out at John Crompton Park in College Station, Texas over a five day period. For each convex polygon created, the Challenge 1 was used to survey the bounded area by both a wind oriented raster scan and the spiral scan. A completed trial was not entered into the final data set unless the two runs were completed back-to-back. This allowed both runs to be affected similarly by the outdoor elements.

Following the completion of 25 complete trials, the above five performance metrics were calculated and statistically analyzed. There was no statistical significance seen for survey time ($p = .59$), survey distance ($p = .061$), or RMS of Cross-track Error ($p = .123$). Although the spiral resulted in a statistically significant lower Hausdorff Distance (1.523535 meters less, $p = .0005$), the wind oriented path plan resulted in a 4.22% increase in percent coverage ($p = .027$). In order to help explain why spiral path plan had such a poor performance in percent coverage, a post-experiment metric Percentage of Locations Inside the Bounding Area was calculated. It was observed that the raster scan had 16.88% higher percentage than that of the spiral scan (p=.00023). It was further seen that the spiral scan only had 34.29% of the outer loops' locations inside the bounded area ($standarderror = .0639$). In conclusion, it can be seen that neither the spiral path plan nor wind oriented raster scan resulted in overall better control of the Challenge 1, but with a statistically significant higher percentage of coverage seen by the raster scan, it can be concluded that the Challenge 1, with its associated controller, should use a wind oriented raster scan to survey a bounded area when performing a radiological survey whose intent is to not only localize a radiological source, but to map its resulting radiological plumes.

7.2 Future Work

Future work for this project falls into three categories: improvements to the spiral like path plan, comparison with a nonholonomic underactuated USV, and extension to radiological sensing-directed spirals. For each of these three categories, an associated subsection is present to elaborate on the needed work.

7.2.1 Path Plan Improvements

Future work for this project would first begin with shifting the spiral's initial outer loop $1/2 \times transectSpacing$ towards the centroid of the polygon. Recall, the initial outer loop of the spiral's path plan was the user defined outer boundary. Shifting the outer loop in would result in all other loops being pushed towards the centroid, but this would still result in a suitable path to survey the bounded area.

After investigating the placement of the initial outer loop, it would be interesting to have the Challenge 1 track its cross-track error throughout the survey in real-time. Then, for any given segment of the survey, the Challenge 1 could check to see if the cross-track error for that segment was above a certain threshold. If it is seen to have exceeded the threshold, the Challenge 1 could backtrack and redo that portion of the survey and adjust the rest of the uncompleted survey accordingly.

7.2.2 Comparison with a Nonholonomic Underactuated USV

The second area of future work for this project consists of applying the spiral-like path plan to other forms of surface vehicle. As mention in this thesis, the Challenge 1 is capable of making turns close to 180 degrees due to its mounted shroud form of force vectoring. Other surface vehicles such as duel propeller vehicles or jet propelled vehicles such as the EMILY offer platforms that could be applied to larger bodies of water with depths and currents not suitable to that of the Challenge 1. Evidence

that the raster scan path plan leads to better autonomous survey's on the Challenge 1 does not prove that it is better for all marine vehicles.

7.2.3 Extension to Radiological Sensing Directed Spirals

Third, it would be beneficial to take radiation readings from the payload in real-time, and use this information to modify the path plan. For example, if areas of water are seen to have radiation readings less than three times the initial background readings, then this section of the water would not need further surveying. This would lead to the unnecessary surveying of areas where no radiation is present and to focus this effort towards higher priority areas. Gino Chacon, a NSF sponsored undergraduate working for the Center For Robot Assisted Search And Rescue lab, has made modifications to the current radiological payload allowing the operator to see the radiation readings in real time. Real-time integration with the payload and path planning module has not yet started.

REFERENCES

[1] Ercan U. Acar, Howie Choset, Yangang Zhang, and Mark Schervish. Path planning for robotic demining: Robust sensor-based coverage of unstructured environments and probabilistic methods. *The International Journal of Robotics Research*, 22(7-8):441–466, 2003.

[2] Esther M. Arkin, Sndor P. Fekete, and Joseph S.B. Mitchell. Approximation algorithms for lawn mowing and milling. *Computational Geometry*, 17(12):25 – 50, 2000.

[3] Prasad N. Atkar, Aaron Greenfield, David C. Conner, Howie Choset, and Alfred A. Rizzi. Uniform coverage of automotive surface patches. *The International Journal of Robotics Research*, 24(11):883–898, 2005.

[4] Volker Bertram. Unmanned surface vehicles-a survey. *Skibsteknisk Selskab, Copenhagen, Denmark*, pages 1–14, 2008.

[5] M. Bibuli, M. Caccia, L. Lapierre, and G. Bruzzone. Guidance of unmanned surface vehicles: Experiments in vehicle following. *IEEE Robotics Automation Magazine*, 19(3):92–102, Sept 2012.

[6] Marco Bibuli, Gabriele Bruzzone, Massimo Caccia, and Lionel Lapierre. Path-following algorithms and experiments for an unmanned surface vehicle. *Journal of Field Robotics*, 26(8):669 – 688, 2009.

[7] Howie Choset and Philippe Pignon. Coverage path planning: The boustrophedon decomposition. In *International Conference on Field and Service Robotics*, 1997.

[8] S. J. Corfield and J. M. Young. *Unmanned surface vehicles - game changing technology for naval operations*. Control, Robotics and Sensors. Institution of

Engineering and Technology, 2006.

[9] Gabriele Ferri, Emanuele Caselli, Virgilio Mattoli, Alessio Mondini, Barbara Mazzolai, and Paolo Dario. Spiral: A novel biologically-inspired algorithm for gas/odor source localization in an indoor environment with no strong airflow. *Robotics and Autonomous Systems*, 57:393 – 402, 2009.

[10] S. Kawatsuma, M. Fukushima, and T. Okada. Emergency response by robots to fukushima-daiichi accident: Summary and lessons learned. *Industrial Robot*, 39(5):428–435, 2012.

[11] Christopher Kitts, Paul Mahacek, Thomas Adamek, Ketan Rasal, Vincent Howard, Steve Li, Alexi Badaoui, William Kirkwood, Geoffrey Wheat, and Sam Hulme. Field operation of a robotic small waterplane area twin hull boat for shallow-water bathymetric characterization. *Journal of Field Robotics*, 29(6):924 – 938, 2012.

[12] Glenn F. Knoll. *Radiation detection and measurement.* New York : Wiley, 2000.

[13] K Kochersberger, K Kroeger, B Krawiec, E Brewer, and T Weber. Post-disaster remote sensing and sampling via an autonomous helicopter. *Journal of Field Robotics*, 31(4):510 – 521, 2014.

[14] K. W. Kratky. The area of intersection of n equal circular disks. *Journal of Physics: A Mathematical and General*, 11(6):1, 1978.

[15] Hans M. Kristensen and Robert S. Norris. Global nuclear weapons inventories, 19452013. *Bulletin of the Atomic Scientists*, 69(5):75 – 81, 2013.

[16] Achim Lilienthal and Tom Duckett. Building gas concentration gridmaps with a mobile robot. *Robotics and Autonomous Systems*, 48(European Conference on Mobile Robots (ECMR '03)):3 – 16, 2004.

[17] Robin Murphy. *Disaster robotics.* Intelligent robotics and autonomous agents. Cambridge, Massachusetts : MIT Press, 2014.

[18] RR Murphy, E Steimle, C Griffin, C Cullins, M Hall, and K Pratt. Cooperative use of unmanned sea surface and micro aerial vehicles at hurricane wilma. *Journal of Field Robotics*, 25(3):164 – 180, 2008.

[19] K Nagatani, S. Kiribayashi, Y. Okada, S. Tadokoro, T. Nishimura, T. Yoshida, E. Koyanagi, and Y. Hada. Redesign of rescue mobile robot quince. In *IEEE International Symposium on Safety, Security and Rescue Robotics*, pages 13–18, Nov 2011.

[20] City of College Station. Ponds. http://www.cstx.gov/index.aspx?page=663, 2016.

[21] K. Ohno, S. Kawatsuma, T. Okada, E. Takeuchi, K. Higashi, and S. Tadokoro. Robotic control vehicle for measuring radiation in fukushima daiichi nuclear power plant. In *IEEE International Symposium on Safety, Security and Rescue Robotics*, pages 38–43, Nov 2011.

[22] M.C.L. Patterson, A. Mulligan, and F. Boiteux. Safety and security applications for micro-unmanned surface vessels. In *Oceans - San Diego, 2013*, pages 1–6, Sept 2013.

[23] Eleonora Saggini, Enrica Zereik, Marco Bibuli, Andrea Ranieri, Gabriele Bruzzone, Massimo Caccia, and Eva Riccomagno. Evaluation and comparison of navigation guidance and control systems for 2d surface path-following. *Annual Reviews in Control*, 40:182 – 190, 2015.

[24] Andrea Sorbara, Andrea Ranieri, Eleonora Saggini, Enrica Zereik, Marco Bibuli, Gabriele Bruzzone, Eva Riccomagno, and Massimo Caccia. Testing the waters: Design of replicable experiments for performance assessment of marine robotic platforms. *IEEE Robotics and Automation Magazine*, 22(3):62 – 71, 2015.

[25] E.T. Steimle and M.L. Hall. Unmanned surface vehicles as environmental monitoring and assessment tools. In *OCEANS 2006*, pages 1–5, Sept 2006.

[26] Seo Sung Mok, Chung Wan Kyun, and Cho Eun Seob. Real time detecting of harmful dinoflagellate cochlodinium polykrikoides using unmanned surface vehicle in dynamic environments. *Journal of Environmental Biology*, 35(3):563 – 570, 2014.

[27] Abhinav Valada, Prasanna Velagapudi, Balajee Kannan, Christopher Tomaszewski, George Kantor, and Paul Scerri. Development of a low cost multi-robot autonomous marine surface platform. In *FSR'12*, pages 643–658, 2012.

[28] G. A. Wilde, R. R. Murphy, D. A. Shell, and C. M. Marianno. A man-packable unmanned surface vehicle for radiation localization and forensics. In *2015 IEEE International Symposium on Safety, Security, and Rescue Robotics (SSRR)*, pages 1–6, Oct 2015.

APPENDIX A

CHALLENGE 1 RADIATION DETECTION SYSTEM*

The Challenge 1 was developed in part through funding by the United States State Department and Sandia National Labs as part of the 2014-2015 Texas A&M's AggiE Challenge project. The project was under the guidance of Dr. Robin Murphy, Dr. Dylan Shell, and Dr. Craig Marianno. The graduate teaching assistant for the project was Grant Wilde. Members who contributed to this project are: Eric Cochrane, Joshua Deitche, Gregory Donelan, Timothy Jacomb-Hood, Ishita Mandhan, Michael Marmo, Daniel Murchison, Rebecca Schofield, and Tianyi Zhang. The Challenge 1 system is composed of the Lutra 1.1 and UltraRadiac Platform, Path Planning, and Interpolation and Visual Heatmap. Each of these systems will be described in further detail below.

A.1 Lutra 1.1 and UltraRadiac Platform

The micro USV used for the data collection vehicle was a Lutra 1.1 autonomous airboat purchased from Platypus, LLC. This surface vehicle has a rudderless design that uses a brushless motor actuated by a servo for propulsion and steering. This design for the USV was chosen due to the absence of underwater propellers. Underwater propellers would limit the micro USV to deep waters that are free of algae or other plants residing at or just below the surface of the water. Since the intended environment in which radiation readings would be collected is mainly in shallow, littoral water, the Lutra 1.1 was the best candidate for the data collection vehicle.

*Part of this section is reprinted with permission from G. A. Wilde, R. R. Murphy, D. A. Shell, and C. M. Marianno. A man-packable unmanned surface vehicle for radiation localization and forensics. In 2015 IEEE International Symposium on Safety, Security, and Rescue Robotics (SSRR), pages 1-6, Oct 2015. Copyright[2015] by IEEE.

The Lutra 1.1 weighs 6.35 kg (14 lbs) with dimensions of 90 x 50 x 45 cm (L x B x H), has a max thrust of 8 N, and has a runtime of 4-8 hours on one battery. However, the payload for the USV can be no more than 2.27 kg (5 lbs). An image of the Lutra 1.1 can be found below.

Figure A.1: The Lutra 1.1 autonomous airboat.

To collect the radiation readings during the boat's survey a Canberra UltraRadiac^{TM}-Plus Personal Radiation Monitor was added to the vehicle. The UltraRadiac^{TM} is a small, rugged, and lightweight sensor that many first responders use when responding to a radiological disaster. The UltraRadiac^{TM} is capable of sensing gamma radiation by employing a windowless Geiger-Muller tube in a range from .0001 micro Gy/hr to 350 cCy/hr with an accuracy of plus or minus 15%. With a weight of only 8.9 ounces (.56 lbs) and dimensions of 10 x 6.6 x 3.1 cm (H x W x D), the UltraRadiac^{TM} was the best candidate for the data collection sensor. The UltraRadiac^{TM} has no internal memory and so is unable to store data locally. It does have an internal infrared port in which the collected data can be transferred to another device in real time. To

account for this, a Netbook with a USB infrared reader was added to read and store all the radiation data that was collected. The output from the UltraRadiac^{TM} is transmitted in a raw text format. A Python script collects data from the infrared port using the pyserial Python module to read the port approximately once per second. Data is parsed to extract the current exposure rate and logged along with system time. This log is then concatenated with the position logs from the Lutra 1.1 using synchronized system time stamps to match exposure rate to its respective GPS position.

The Lutra 1.1 comes equipped with two transportation modes: 1) tele-operation mode and 2) autonomous mode. The tele-operation mode allows the user to send a thrust and a heading to the boat. The autonomous mode supports three operation modes: 1) point, 2) path, and 3) area. Point mode allows the user to select a point on the map in the user interface and the boat will traverse to that point. Path mode allows the user to select a series of points in the user interface that the boat will traverse to in order. Area allows the user to select the boundary points of a convex or concave polygon in the user interface in which the USV will autonomously search the area inside the polygon via a lawnmower path plan. Since the approach taken in this paper is to allow the user of the USV to tele-operate and mark each intended boundary point, the open source software for the Lutra 1.1 operator interface had to be changed. The "New B.P." button was added to allow this functionality. This new button writes the boat's current position to memory so that the current location can become a new boundary point to the user defined convex polygon. During boundary point marking, the operator can use either the tele-operation mode to traverse to the next intended boundary point or use point mode to traverse to the next boundary point. Once at the location of interest, the user then clicks the "New B.P." button to write the location to memory. The last modification made to the operator interface

source code was the implementation of a customized log file. The log file created upon connection to the boat writes timestamp, latitude, and longitude to a file. As mentioned earlier, this log file can then be concatenated with the log file created from the onboard UltraRadiac^{TM} payload.

A.2 Path Planning Module

As stated above, the Lutra 1.1 comes with the ability to autonomously search an area inside a user defined convex polygon via a lawnmower path. For the initial testing of this system, a lawnmower path will not guarantee radiation readings are taken along a line parallel to the convex polygon's edges. Therefore, a new path planning algorithm was implemented so a spiral-like path is taken. A spiral-like path reduces the need for the USV to complete multiple 180 degree turns that the USV would have to make if a lawnmower path was executed. The idea is that the original polygon that is created by the operator, as described above, forms the outer loop of the spiral and is added to a new list of points forming a new polygon. To create the next inner loop of the path, each previous boundary point from the newly created polygon is moved a fixed, user defined distance d towards the centroid of the polygon forming a new potential location. Before being added to the final path, the distance from this new location to the centroid of the polygon is calculated. If this distance is less than d, it is not added to the path, otherwise the location is added to the list of points to traverse. After each of the locations of the polygon has been adjusted and checked against the centroid, the old polygon is deleted and the newly created locations are used to form the next, new polygon. This process is repeated until the polygon is decreased to a line, i.e. two points. Once two points remain, the process is terminated and the centroid of the original polygon is added to the path to insure complete coverage of the user defined area. Upon completion of the final path, the

list of coordinates generated is sent to the boat instead of the lawnmower path the software would have generated otherwise. With this said, no hardware or software was modified on the USV's onboard system.

The above path planning algorithm was seen to have transects that were neither parallel nor equidistant to previous transects. To combat this, the spiral-like path plan was re-written as to combat this issue. Further explanation of the new spiral path plan will be given in a subsequent section.

A.3 Interpolation and Visual Heatmap

The visual heatmap system has three main components: 1) communication, 2) interpolation, and 3) Google Earth overlay. Each of the components can be used independently or together in a sequence to provide the mission specialist with a visual heat map. The communication module is used to provide real-time data transmission through Java Sockets. The interpolation module is written as a Python script with four main interpolation algorithms as functions: 1) simple kriging, 2) ordinary kriging, 3) radial basis function, and 4) inverse distance weighting. Google Earth is used to overlay the heatmap from the interpolator on a geographical region. For the purposes of this thesis, the real-time data transmission was not used. Instead, all data was collected then analyzed post survey.

As soon as the data collection has been terminated, the log file generated on the control end containing timestamp and GPS location is joined with the log file generated by the onboard UltraRadiac^{TM} payload containing timestamps and radiation readings. A Python script is used to accomplish this task and outputs a .csv file with each line of the file having the form "latitude, longitude, radiation reading". Next the data are passed to one of the four interpolation algorithms which in turn, creates a .png of the heatmap. Once the heatmap has been created it is then overlayed on

the geographical region within Google Earth.

A.4 Demonstration

The full scale test of the described USV radiation localization system took place on May 12, 2015, at one of the ponds at Texas A&M Engineering Extension Service's (TEEX) Disaster City® in College Station, Texas. Disaster City® is a 100-acre training facility that features collapsed buildings, rubble piles, derailed trains, and many other simulated disaster scenarios. For the purposes of this field test, a cesium-137 radiological source was placed on the southeast bank approximately 2 meters from the water's edge (see Figure A.2 and 72 meters from where the USV was deployed. As this was an initial test, the distance was relatively short and the USV stayed in line of sight. The radiological source was transported to Disaster City® by Texas A&M's Environmental Health and Safety's radiological safety unit, meeting all the regulations and requirements imposed by the United States and the State of Texas's governments.

Figure A.2: The yellow star indicates where the cesium-137 source was placed and the blue circle indicates where the USV was deployed.

The intent of this demo was to demonstrate and test each of the major modules of the USV system. For the complete system to be successful, the following four modules had to be completed:

1. Specification of safe navigation polygon via telo-peration
2. Path generation and execution
3. Radiological data collection
4. Generation of interpolation and visual heat map

The process of completing the above modules begins with the Lutra 1.1 safely navigating to each of the user defined boundary points, via tele-operation, and saving these boundary points to memory. The boundary points are saved to the same laptop that is acting as the operator control unit (OCU). Once the boundary point marking phase is complete, the resulting polygon is then passed to the getPath() function. After the getPath() function generates a list of GPS coordinates that the USV is to traverse, these coordinates are sent to the USV in the water. Upon receiving the generated path from the controller, the Lutra 1.1 then autonomously traverses to each of the desired coordinates while simultaneously collecting radiation readings. The operator is notified that the path execution is complete when the fan on the USV turns off and the path in the Operator Interface disappears. After the survey has been completed and the USV is safely out of the water, the data from the onboard UltraRadiac^{TM} payload is transported to the OCU laptop via a USB flashdrive, and is then joined with the GPS log file created by the OCU with the common key being timestamp. This process is completed by a Python script that outputs a .csv. This .csv is then transferred to a data analysis laptop where the interpolation and heat map creation takes place. The complete process can be seen in Figure A.3.

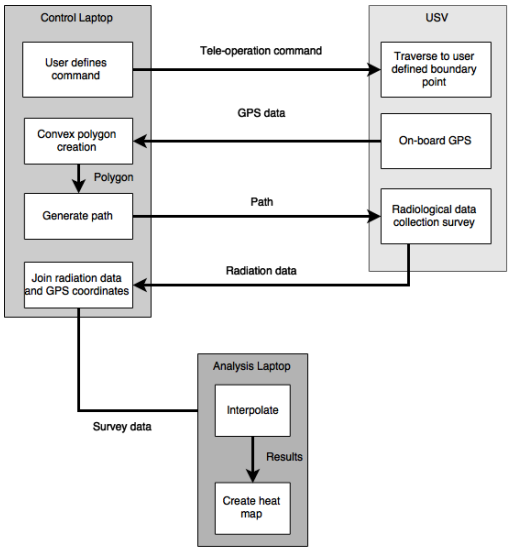

Figure A.3: The complete data collection process.

A.5 Results

The weather conditions for College Station on May 12, 2015 were overcast with scattered showers. Due to these unfavorable weather conditions, only one trial was executed. The trial lasted 18 minutes and 19 seconds. However, the trial was sufficient to demonstrate the unique algorithms used in the system: creation of boundaries via teleoperation, spiral path planning and generation, and the interpolation and heat map.

A.5.1 Polygon via teloperation

The user defined convex polygon was successfully created by marking 9 boundary points. The operator used the Lutra 1.1's point autonomous mode to traverse to each of the desired points, then clicked the "New B.P." button to mark the boundary point. The area covered by the polygon was 21.58 square meters and can be seen in Figure A.4.

A.5.2 Path generation and execution

In the figure below, the generated path the USV was given is shown as it appeared in the Operator Interface (Figure A.4a). The spiral path was generated in less than one second and generated 17 waypoints. The runtime of the getPath() function was calculated by logging the system time before and after the call to the getPath() function. The resulting timestamps were identical, therefore resulting in a runtime of less than one second. Notice the path planning algorithm did not fully complete its execution. This software error has since been corrected and the new path plan is shown as it would appear in the Operator Interface (Figure A.4b). The new path generated 26 waypoints to traverse and was generated in less than one second as well. This path was generated with the exact same boundary points as Figure A.4a but has not been tested with the USV and radiation source at this time.

(a) Generated and executed path.

(b) Corrected path.

Figure A.4: Figure A.4a shows the actual path plan that was sent to and executed by the USV. Figure A.4b shows the correct path generation that has yet to be tested with a radiological source.

The Lutra 1.1 traversed the yellow path shown in A.4. The portions of the path on land are due to the fact that the Lutra 1.1 was connected to the Operator Control Unit on land, and carried by hand to and from the water. The execution of the generated path took 8 minutes and 4 seconds. This time was determined by measuring the time the motor turned on to begin the path traversal to the time the motor shut off after completing the path.

Figure A.5: The yellow portion indicates where the USV traveled. The red polygon shows the intended area formed after marking the 9 boundary points via teleoperation.

A.5.3 Radiological data collection

Once the log file created by the onboard UltraRadiac^{TM} was transferred via a USB flashdrive to the Operator Control Unit and joined to the log file created by the OCU, a .csv file containing "latitude, longitude, radiation reading" was interpolated using the inverse distance weighting method to form the heat map shown in Figure A.6. In total, 775 radiation readings were taken, with approximately .705 collected

samples per second. The minimum radiation reading was 0 micro R/hr and the maximum radiation reading was 75 micro R/hr.

A.5.4 Interpolation and Heat Map

The heat map created in Figure A.6 had an overall area of 57.61 square meters. In general, there is no set interval to determine a radiological heat map's color scheme. Color schemes are event specific based on radionuclide and exposure rate. For this demonstration the areas in green show areas that had an interpolated radiation reading between 0 micro R/hr to 39 micro R/hr. Areas in yellow show regions with an interpolated radiation reading between 40 micro R/hr to 79 micro R/hr. Though not present on this heat map, areas of orange would indicate regions with interpolated radiation readings between 80 micro R/hr to 119 micro R/hr and areas of red would indicated regions with interpolated radiation readings greater than or equal to 120 micro R/hr.

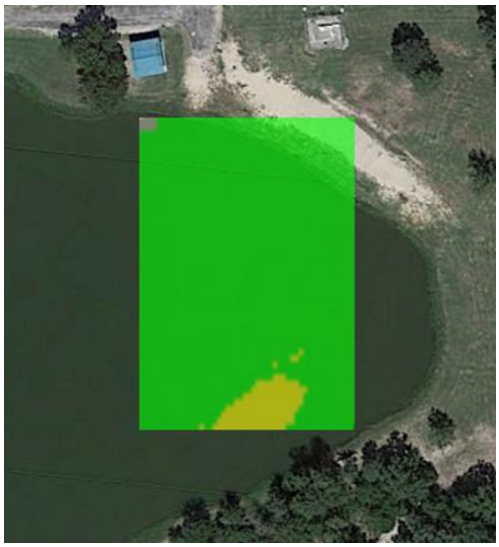

Figure A.6: The green area shows areas that had interpolated radiation readings between 0 to 39 micro R/hr and the yellow area shows regions with interpolated radiation readings between 40 to 79 micro R/hr.

APPENDIX B

WIND PARAMETERS, DIRECTIONS, AND SPEEDS

This section includes all the operator entered wind parameters used for the wind oriented raster scan as well as the wind directions and speeds recorded prior to and after each successful run. Wind speed was measured using a Ambient Weather WM-2 Handheld Weather Meter. The wind direction was noted from the The Weather Channel IPhone application, and was verified using the wind meter and compass on said IPhone. A minimum wind reading of .4 miles per hour was recorded and a maximum of 7.7 miles per hour was recorded.

Trial	Path Plan	Wind Parameter (degrees)	Wind Direction Before Run	Wind Speed Before Run (mph)	Wind Direction After Run	Wind Speed After Run (mph)
1	Raster	67.5	SSE	2.4	SSE	3.7
	Spiral	N/A	SSE	3.4	SSE	1.0
2	Raster	67.5	SSE	3.2	SSE	5.3
	Spiral	N/A	SSE	4.4	SSE	6.0
3	Raster	67.5	SSE	4.2	SSE	5.3
	Spiral	N/A	SSE	3.6	SSE	4.6
4	Raster	67.5	SSE	1.9	SSE	4.0
	Spiral	N/A	SSE	4.7	SSE	3.2
5	Raster	67.5	SSE	4.7	SSE	5.1
	Spiral	N/A	SSE	4.9	SSE	4.7
6	Raster	90	S	5.9	S	4.5
	Spiral	N/A	S	7.5	S	5.0
7	Raster	90	S	4.1	S	3.6
	Spiral	N/A	S	2.5	S	6.0
8	Raster	90	S	2.5	S	2.9
	Spiral	N/A	S	3.8	S	1.0
9	Raster	90	S	5.2	S	2.7
	Spiral	N/A	S	2.4	S	4.3
10	Raster	90	S	1.8	S	1.0
	Spiral	N/A	S	3.2	S	2.8
11	Raster	45	NW	2.4	NW	5.1
	Spiral	N/A	NW	2.2	NW	2.4
12	Raster	45	NW	1.5	NW	3.1
	Spiral	N/A	NW	2.8	NW	2.1

Table B.1: Wind parameters, directions, and speeds for Trials 1-12

Trial	Path Plan	Wind Parameter (degrees)	Wind Direction Before Run	Wind Speed Before Run (mph)	Wind Direction After Run	Wind Speed After Run (mph)
13	Raster	45	NW	1.7	NW	2.0
	Spiral	N/A	NW	1.5	NW	3.9
14	Raster	45	NW	2.2	NW	4.5
	Spiral	N/A	NW	4.8	NW	6.0
15	Raster	45	NW	3.9	NW	1.2
	Spiral	N/A	NW	7.7	NW	5.5
16	Raster	112.5	SSW	3.3	SSW	3.6
	Spiral	N/A	SSW	4.7	SSW	2.4
17	Raster	112.5	SSW	3.9	SSW	1.9
	Spiral	N/A	SSW	4.5	SSW	1.1
18	Raster	0	W	2.8	W	1.6
	Spiral	N/A	W	4.8	W	4.2
19	Raster	0	W	4.5	W	.5
	Spiral	N/A	W	3.4	W	.4
20	Raster	0	W	1.2	W	2.9
	Spiral	N/A	W	2.1	W	1.4
21	Raster	67.5	SSE	2.1	SSE	2.2
	Spiral	N/A	SSE	5.5	SSE	4.6
22	Raster	67.5	SSE	1.4	SSE	4.2
	Spiral	N/A	SSE	4.3	SSE	4.9
23	Raster	67.5	SSE	2.3	SSE	4.6
	Spiral	N/A	SSE	7.5	SSE	4.7
24	Raster	67.5	SSE	4.8	SSE	4.7
	Spiral	N/A	SSE	4.5	SSE	5.2
25	Raster	22.5	ESE	5.8	SSE	5.3
	Spiral	N/A	ESE	5.9	SSE	6.0

Table B.2: Wind parameters, directions, and speeds for Trials 13-25